

# **Work Package 8**

## **Deliverable 8.4**

EISCAT-3D as a geophysical observatory:

Instruments, data types, data combination  
and implications for data system design.

Ian McCrea, Derek McKay and Ivan Finch

## Contents: Deliverable 8.4

1.	Introduction	p4
2.	EISCAT-3D as an observatory	5
3.	Candidate instruments for an STP observatory	10
3.1	Other Types of Radar	10
3.1.1.	HF and VHF coherent scatter radars	10
3.1.2	MST radars	12
3.1.3	Meteor scatter radars	14
3.1.4	Partial reflection and API experiments	16
3.1.5	Magnetospheric radars	17
3.2	Ionospheric sounders	17
3.2.1	Ionosondes	17
3.2.2	HF Doppler systems	19
3.2.3	Oblique sounders	20
3.3	Lidars	21
3.4	Passive optical imagers	23
3.4.1	Auroral imagers	23
3.4.2	All-sky imagers	24
3.4.3	High resolution auroral imagers	25
3.4.4	Airglow imagers	26
3.4.5	Fabry-Perot interferometers	27
3.4.6	Photometers	28
3.4.7	Radiometers	29
3.4.8	Spectrometers	29
3.5	Passive radio instruments	29
3.5.1	GPS and beacon satellite receivers	30
3.5.2	Riometers	31
3.5.3	VLF and ELF receivers	32
3.6	Magnetometers	33
3.6.1	Fluxgate magnetometers	33
3.6.2	Proton precession magnetometers	34
3.6.3	Pulsation magnetometers	34
3.7	Ionospheric heaters	35
4.	Existing facilities and EISCAT-3D requirements	36
4.1	Other types of radar	36
4.2	Ionospheric sounders	38
4.3	Active optical instruments	38
4.4	Passive optical instruments	39
4.5	Passive radio instruments	41
4.6	Magnetometers	41
4.7	Summary	41
5.	Infrastructure and data rate implications	42
5.1	Supporting instruments at the central site	43
5.1.1	Other types of radar	43
5.1.2	Ionospheric sounders	45
5.1.3	Active optical instruments	46
5.1.4	Passive optical instruments	46
5.1.5	Passive radio instruments	48
5.1.6	Magnetometers	49

5.2	Supporting instruments at the remote sites	49
5.3	Summary of data rates and infrastructure requirements	50
5.4	Discussion	53
6.	Data combination and value-added products	53
6.1	Calculation of vector velocity	54
6.2	Ion-neutral difference velocity	55
6.3	Electrodynamic parameters	55
6.4	Neutral temperatures	56
6.5	Ion and neutral composition	56
6.6	Heat flux, suprathermal electrons and plasma lines	57
6.7	Potential patterns	57
6.8	Energy maps	58
6.9	Tomographic images and their calibration	58
6.10	The importance of models	59
7.	Data distribution techniques	61
8.	Metadata in EISCAT-3D	63
9.	Data, users and services	65
10.	Summary and conclusions	69
	References	71

## **1. Introduction**

This report constitutes the fourth deliverable from Work Package 8 of the EISCAT-3D design study. In the previous deliverables from this Work Package, we have concerned ourselves purely with the various data products produced by the EISCAT-3D radars themselves, namely the raw beam-formed voltage level data, the auto-correlated data (integrated both temporally and spatially), the summary analysed data, the interferometric data (visibility functions or derived brightness patterns) and the engineering metadata, comprising both system status data and data relating to external factors such as interfering signals.

In Deliverable 8.3 (published September 2008) we set out a detailed topology for the data system needed to handle these various data products, together with the required network speeds and storage capacities at each stage which were needed to ensure that data could be handled according to our original design concept. We showed that this concept, although challenging, could already be realised with existing 2008 technology, and provided examples of real-world hardware solutions which could be deployed to meet our criteria, based on extensive discussions with a number of commercial vendors of storage and computing equipment.

However, our concept of EISCAT-3D is that it should be more than simply a radar facility. This idea is founded on our long existing experience of operating the EISCAT radars and working with their user communities, and our perception of developments at other incoherent scatter radars worldwide. We have found that these highly-capable radars invariably act as magnets to attract a whole variety of supporting instrumentation, using a wide range of diagnostic techniques. Many of these co-located supporting instruments are individually small, and certainly very much less expensive than the ISRs. In general, such diagnostics are owned and operated by particular research groups or consortia of groups, who also use the main radar and wish to combine or compare the radar data with those from the other instruments. This is a very logical requirement, since much of the science done in Solar-Terrestrial Physics is inherently multi-diagnostic, based on the use of multiple data sets from instruments each of which is capable of probing the solar-terrestrial system in a different way. This could mean other radars at different wavelengths, optical imagers of various types, magnetometers, riometers, HF sounders and many others. A complete list of possible types of observing systems is given in Section 4.

Up to now, the supporting instruments operating in conjunction with the incoherent scatter radars have mainly been deployed in an ad-hoc manner. This means that the planning and initial construction of the radar site and its infrastructure has in general made no prior allowance for the arrival of supporting instruments, which has meant that the groups responsible for these systems have been forced to make their own arrangements for accommodating support instruments and coping with their data. This is certainly the situation with the instruments currently deployed in conjunction with EISCAT.

The EISCAT-3D project will essentially be a "green field" development, and this allows us to plan for the development of the radar sites and their supporting infrastructure in such a way that the requirements of these supporting instruments are already built in. As well as obvious requirements such as space to deploy

instruments, domes for optical sensors etc, one of the largest potential impacts of having a number of supporting instruments on site will be the implications for the data system, explaining why this area has been assigned as a WP8 responsibility.

In this report, we discuss the concept of operating the EISCAT-3D radar sites as multi-purpose STP observatories. We have surveyed the current situation at comparable installations around the world, looking at the types of instrument which have been deployed and operated in conjunction with the other radars and STP facilities. For each possible type of supporting instrument, we briefly review the standard modes of operation and the data and volume of data produced in each mode. We discuss the potential requirements for each type of data product to be post-processed, and examine whether such post-processing needs to be done locally and whether it results in an increase or decrease in data volume. We also examine the potential for combining data from multiple instruments into new value-added data products, and comment on the desirability of including these products in the final suite of data products produced by EISCAT-3D and held in its central archive.

Having done these things, we are able to provide a first order estimate of the amounts of data which will be produced by the supporting instruments operating in conjunction with EISCAT-3D. In describing these data, we distinguish between those data sets which might only need to be stored for a short time in order to be processed into more compact and permanent data products, and those which need to be added into a permanent data archive.

This does not necessarily imply that we regard the data handling for all these instruments as being the responsibility of the EISCAT-3D project. Indeed, we anticipate that (as now) the costs of operating such instruments can continue to be shared between the institutions responsible for operating them. Forcing each instrument provider to make their own arrangements for data storage and distribution, however, implies a considerable duplication of effort. The point of undertaking this exercise as part of the design study is so that these requirements can be factored into the design of the common EISCAT-3D infrastructure, even if the implementation is ultimately realised by a collaboration involving the instrument providers. The result is an elaboration of the basic data system design proposed in D8.3, which will ensure that the network, storage and processing capacity available at the EISCAT-3D sites will be sufficient for all of the various instruments which, we anticipate, will be deployed there.

## **2. EISCAT-3D as an observatory**

Although incoherent scatter radars are extremely powerful tools, it has to be recognised that they are only capable of measuring a relatively small subset of the parameters accessible to the full range of STP instruments, so that data from these other instruments are often essential for putting the incoherent scatter data into their correct physical context. Figure 1 (from Lunde et al, 2007) shows a time series of incoherent scatter spectra measured using the EISCAT Svalbard Radar. ESR spectra mainly comprise the symmetric, double-humped forms characteristic of thermal incoherent backscatter, but notable deviations are seen during short-periods when one or other spectral wing becomes very enhanced with respect to the other, resulting in highly asymmetric non-thermal spectra. While such an observation would be

extremely interesting in its own right, a physical interpretation is not possible using incoherent scatter radar data alone. The explanation of this phenomenon is only possible by comparing the spectra with simultaneous data from a multi-wavelength auroral camera.

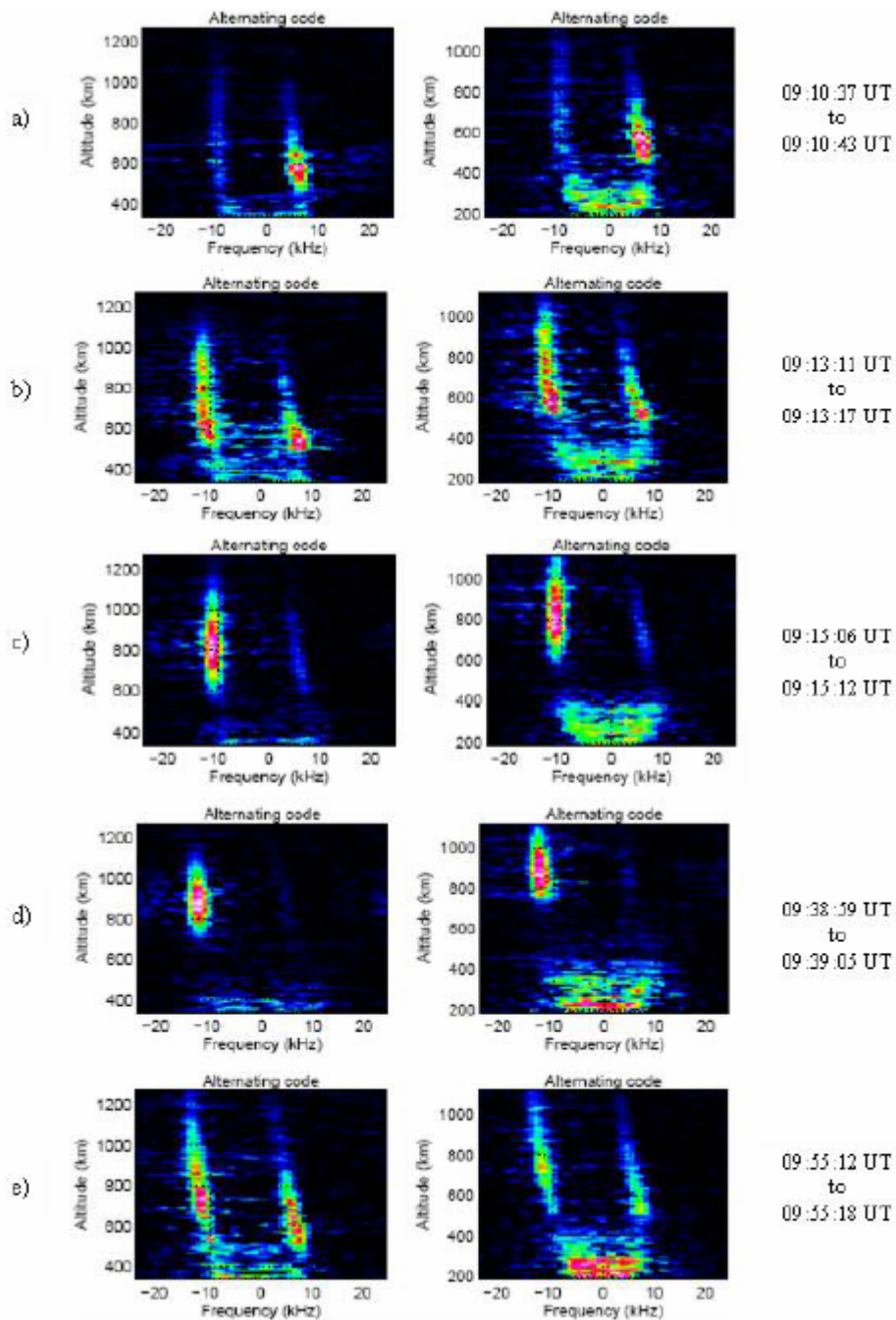


*Figure 1: Time series of incoherent scatter spectra from the EISCAT Svalbard Radar, from January 22 2004, showing the asymmetric forms characteristic of Naturally Enhanced Ion Acoustic Lines (NEIALs) (Lunde et al, 2007)*

Figure 2 from the same paper illustrates that the times at which asymmetric spectra were observed correlate precisely with periods when highly-structured auroral arcs were present in the EISCAT beam, while optical data obtained by Sullivan et al (2008) have also shown that these structures are seen most strongly in red-line auroral

emission, suggesting that the process responsible for these structures is driven by some of the lowest-energy electrons. The full interpretation, that the anomalous spectra are produced by the collapse of Langmuir waves into ion-acoustic waves, driven by free energy from low energy precipitation, can therefore only be made by the combination of radar and optical data.

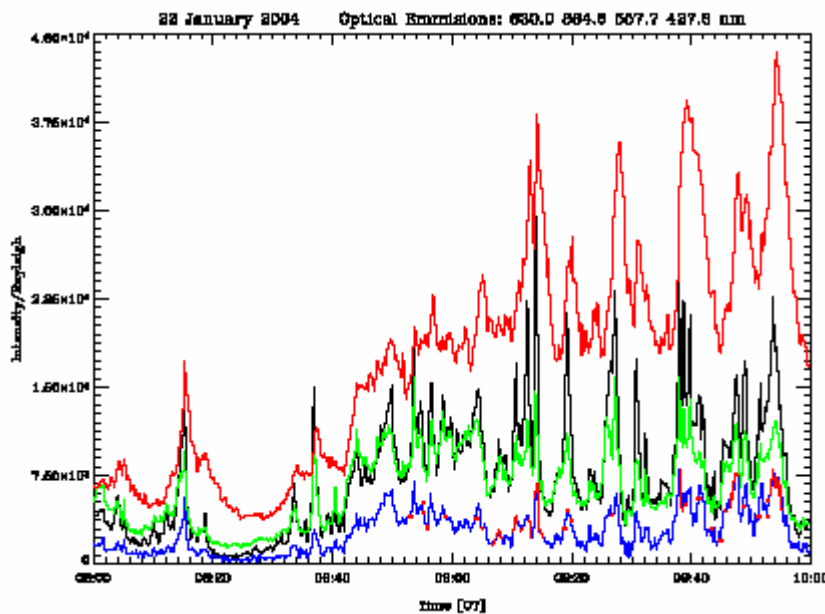


Figure 2: Simultaneous multi-wavelength optical intensities from January 22 2004. The peaks in emission intensity correspond well with times of NEIAL activity (Lunde et al, 2007)

As another example, consider the data shown in Figure 3, taken from a paper by Belova et al (2005). The centre panel shows data obtained during an intense solar proton event which occurred in October 2003, and show a dramatic increase in the low-altitude electron density observed at EISCAT, due to increased ionisation caused by a large enhancement in the solar soft X-ray flux. Embedded within the region of enhanced ionisation, however, is a narrow intense layer within which the backscatter cross-section has increased by two orders of magnitude with respect to that of the background plasma. The top panel shows another simultaneous data set, obtained from the ESRAD 50 MHz radar, located about 100 km to the South-East of EISCAT, at Andøya. These data show the same layer as seen by the EISCAT VHF radar, but with somewhat different features, with an apparently smaller power enhancement and a narrower scattering region. The bottom panel shows the Doppler velocity measured by EISCAT, with the location of the PMWE layer marked by solid lines

The enhanced D-region density in this event was confirmed by the large increase in ionospheric absorption, shown in the top panel of Figure 4, as measured by the reduction in Cosmic Noise measured by the IRIS riometer at Kilpisjärvi in Finland (Friedrich et al, 2006). Figure 3 also shows the electron densities from the EISCAT VHF radar (second panel), the modelled electron density variation for this interval (third panel) and the discrepancy between the radar data and the model (bottom panel). At the same time, data from the EISCAT UHF radar showed no sign of the intense density feature seen by the VHF, and data from the Tromsø magnetometer

showed that there was no corresponding magnetic signature, suggesting that this feature was not auroral.

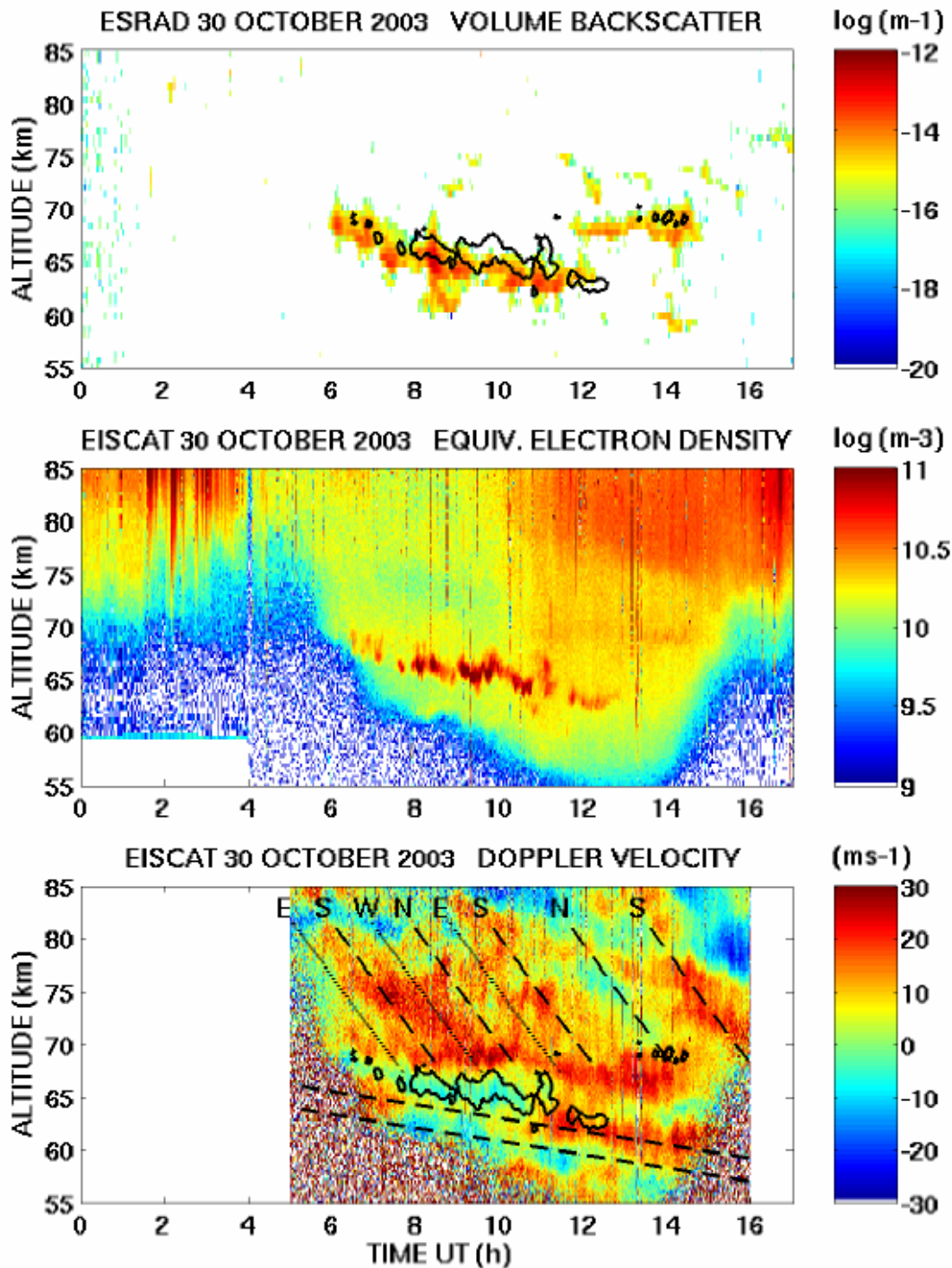


Figure 3: Simultaneous results from the ESRAD MST radar (top panel) and the EISCAT VHF radar (middle and lower panels) showing backscatter power and Doppler signatures during the intense PMWE layers of October 30 2003 (Belova et al, 2005).

The combination of all these data resources allowed the authors to come to the optimal interpretation of this event, namely that this observation was consistent with a so-called PMWE (Polar Mesosphere Winter Echo) event, in which the 64 cm

wavelength ion-acoustic waves sensed by the EISCAT VHF were being fed by the decay of longer-wavelength turbulence, probably originating in the neutral atmosphere, which is sensed by the 50 MHz radar. However this decay to shorter wavelength structures had been quenched before the energy enhancement reached the 16cm ion-acoustic waves sensed by the EISCAT UHF radar.

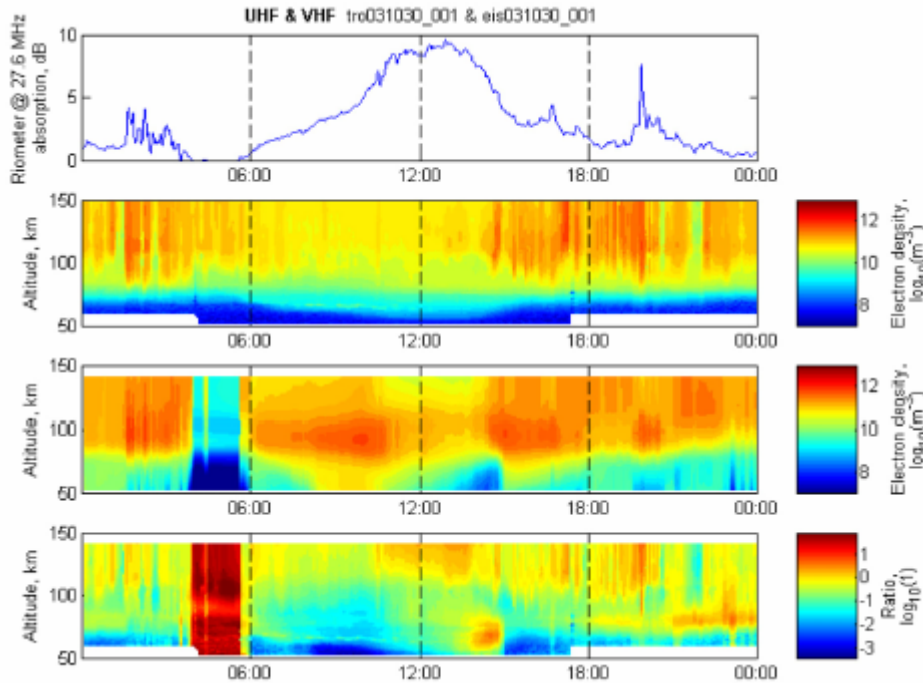


Figure 4: Simultaneous riometer (top panel), EISCAT VHF (second panel) and model predictions (third panel) for the events of October 30 2003. The bottom panel represents the discrepancy between the EISCAT data and the model (Friedrich et al, 2006).

One could provide many more examples in which the interpretation of incoherent scatter radar data can only be performed with the addition of other simultaneous data sets and models. However the main point of this section is to stress that this kind of multi-diagnostic data use is the norm, rather than the exception. The majority of research papers using data from incoherent scatter radar data also use data from one or more other type of diagnostic, and many of these diagnostics are co-located ground-based instruments.

What this means is that the EISCAT-3D radar sites should not be designed purely to accommodate the radar facilities. Rather, they should be designed as STP observatories, capable of hosting a wide variety of other instruments. This means that the sites should provide not just physical housing for such instruments, but also provide sufficient data processing, storage and transport capacity to enable the data from these instruments to be handled for at least their appropriate standard processing and for the derived data products to be removed from the site, preferably to a permanent central archive. Since WP8 is already charged with developing the basic infrastructure of the EISCAT-3D data system, it is obvious that we should look into the requirements for extending the data system to handle the data from these other instruments also, as part of the common underpinning infrastructure of the radar sites.

### **3. Candidate Instruments for an STP Observatory**

In this section, we briefly review the most commonly-occurring diagnostic instruments which are either already deployed in support of ISRs, or might be deployed in the near future. For each type of instrument, we look at the basic data products, the data rates involved, the possibilities of post-processing the data and the requirements for long-term and short-term data storage. We also examine the likelihood that such instruments will actually be deployed at the EISCAT-3D sites, given the existing complement of instruments which are deployed in mainland Scandinavia.

#### **3.1 Other Types of Radar**

Apart from their size and complexity, the main factor which differentiates incoherent scatter radars from other types of radar is their wavelength, which in turn determines the type of irregularity from which backscatter occurs. The presence or absence of such irregularities further determines the region of the atmosphere which can be probed using these techniques, and constrains the kind of science which can be done with their data. Here we discuss five different types of radars, namely coherent scatter radars, MST radars, meteor scatter radars, magnetospheric radars and partial reflection/API experiments. In general these different radar techniques are highly complementary to each other, so that there are multiple examples where different types of radars are deployed on the same site, or with the same coverage area.

##### **3.1.1. HF and VHF Coherent Scatter Radars**

Coherent scatter radar, like incoherent scatter radar, is a volume scattering technique in which the radar detects energy scattered from within a medium when there are regular spatial variations of the refractive index due to irregularities. The terms "coherent" and "incoherent" scatter are used rather loosely in the atmospheric radar community, and the difference between the two techniques lies mainly in the stability of the scattering structures. In the case of incoherent scatter, the scattering irregularities are ion-acoustic waves, which are short-lived fluctuations generally only coherent on timescales of less than a few milliseconds. Beyond this time, samples of the same scattering volume are unrelated in phase and amplitude - however as long as the underlying medium does not change, the autocorrelation functions obtained from these scattered samples have the same statistical properties, and can be added.

In coherent scatter radars, however, the scattering structures are much longer-lived electron density corrugations with amplitudes of order 5%, which are generally aligned with the magnetic field and which occur on scales from centimetres to tens of metres. Scattering from these irregularities is analogous to Bragg scattering in crystals, in that signals backscattered from plasma wave irregularities with a spacing of half the radar wavelength will reinforce by constructive interference in the direction back to the radar and can produce a signal strong enough to be detected by the receiver. Hence using a particular radar wavelength picks out a particular wavelength of irregularity, even if structure in the plasma exists over a wide range of wavelengths.

One strength of the coherent scatter technique is that multiple radars at different frequencies can be used simultaneously to probe different irregularity wavelengths which occur in different height regions of the ionosphere. For example, VHF coherent scatter radars such as STARE are sensitive to field-aligned density irregularities in the E-region, while HF coherent scatter radars such as CUTLASS are sensitive to longer-wavelength field-aligned irregularities, which mainly occur in the F-region. In the case of HF radars, the refraction of the ray path in the ionospheric plasma is a major factor in producing the orthogonality between the radar k-vector and the magnetic field which is required for the detection of backscatter. In HF radars, the orthogonality condition is satisfied at a number of discrete ranges, corresponding to various allowed propagation paths (e.g. half hop, single hop, 1.5 hop). In VHF coherent scatter radars, orthogonality is usually only satisfied at one range per beam direction; and because these frequencies are not affected by refraction, the important factor is purely the orientation of the illuminating radar beam. In the case of HF coherent scatter radars, the frequency range generally used for coherent scatter is from around 5 to 15 MHz, while VHF coherent scatter radars generally exploit the range 50 to 200 MHz, though coherent backscatter from field-aligned irregularities has been detected all the way up to frequencies of 1.2 GHz.

Unlike incoherent scatter radar, there is no robust theory linking the spectral power and shape of the received coherent scatter signal to the underlying plasma parameters. Also coherent scatter tends not to be continuous in range, because of the need for the signal propagation to satisfy the orthogonality conditions referred to above. Finally, the density irregularities responsible for coherent scatter are intermittent, in that they only occur when appropriate threshold conditions have been exceeded (e.g. relating to the underlying electron density and electric field strength). This means not only that it is not possible to derive plasma parameters such as electron density and temperature from coherent scatter radar data, but also that there are frequent intervals where no data can be obtained from radars of this type because the scattering irregularities are simply absent. Nevertheless, because coherent scatter radars are robust, relatively cheap and run automatically in standard modes, networks of such radars have become a very important tool in geophysics.



*Figure 5: The Iceland East SuperDARN radar at Stokkseyri (from the SuperDARN web site).*

The SuperDARN network (<http://superdarn.jhuapl.edu/>) currently comprises 12 coherent scatter radars in the northern hemisphere and 7 in the southern hemisphere, with radars whose viewing areas cover both auroral zones from a wide range of longitudes. The viewing areas of the SuperDARN radars are very large, because of their ability to transmit and receive data from a wide fan of multiple near-simultaneous beams, and the overlap between the different ranges means that SuperDARN has observational coverage across much of the auroral zone and polar cap in both hemispheres.

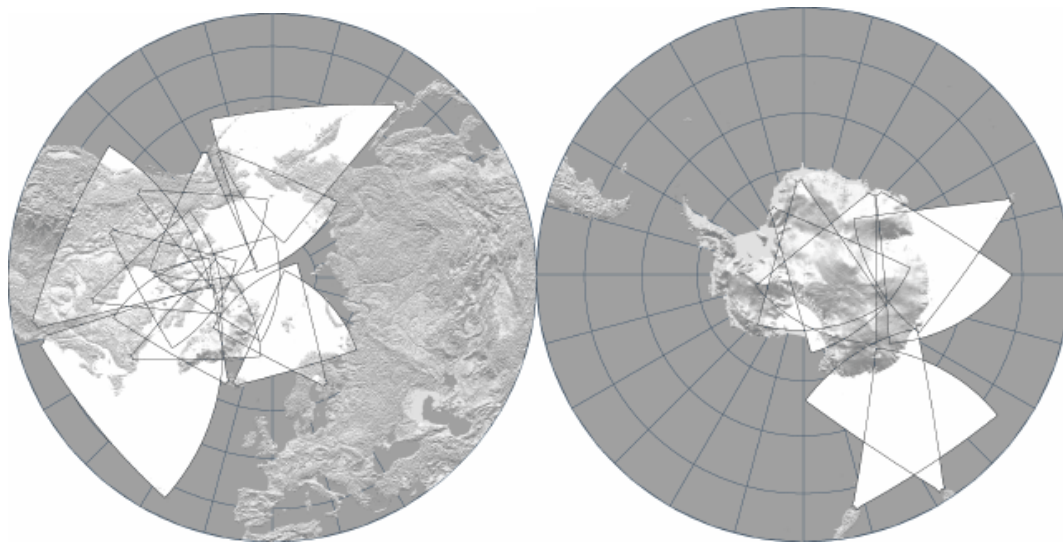


*Figure 6: Northern and southern hemisphere coverage of the SuperDARN network (source, SuperDARN web site).*

Recently, the coherent scatter community has been pursuing two major enhancements to the SuperDARN network. StormDARN is an equatorward extension of the SuperDARN network, currently consisting of two radars in the American sector to study how high-latitude electric fields penetrate to lower latitudes during storm-time conditions. PolarDARN is a northward extension of the network, also currently comprising two radars in the US sector, to cover the northern polar regions. The radars used by StormDARN and PolarDARN are identical to those used by SuperDARN, and in reality both extensions represent an expansion of the international coherent scatter radar network.

### 3.1.2. MST Radars

Mesosphere-Stratosphere-Troposphere (MST) radars are mainly designed for probing the lower atmosphere, and are optimised to scatter from the troposphere and lower stratosphere. The frequency of such radars is normally around 50 MHz (though frequencies around 400 MHz and 1 GHz are also used), and the returned signal tends to come from two distinct altitude regions. In the lower atmosphere (2 to 20 km altitude) the scatter comes from irregularities in atmospheric refraction, also known as "clear-air turbulence". There is then a considerable gap in coverage, until altitudes are reached at which free electron scatter from the mesosphere becomes possible (generally in the altitude region 55 to 90 km). Mesospheric scatter is normally seen only by the lower-frequency MST radars, and is often treated as a rather incidental by-product of the more interesting lower atmosphere data, although some radars place

considerable importance on the study of mesospheric phenomena. MST radars are also capable of receiving meteor scatter, though the study of such scatter is dealt with in the next section. Also included in this class of radars are the so-called "wind profilers", compact radar systems for the study of lower atmosphere winds, usually operating in the frequency range between 400 and 900 MHz. At polar latitudes, the usefulness of MST radars is enhanced by their ability to detect Polar Mesosphere Summer Echoes (PMSE) and Polar Mesospheric Winter Echoes (PMWE), whose nature and occurrence are of considerable interest to atmosphere and climate scientists (see the Science Case discussion in Deliverable 8.3).



*Figure 7: The UK MST radar at Capel Dewi, mid-Wales (from the NERC MST radar facility web site <http://mst.nerc.ac.uk/IMAGES/>).*

MST radars tend to be ground-mounted Yagi arrays, with capabilities for both beam steering and phase coding/decoding of the transmission and reception, since altitude resolution is an important requirement. Measurements are usually made sequentially in three or more non-coplanar directions to recover vector information about atmospheric velocity. The scatter is continuous over a broad range of altitudes (though not the whole range up to the mesosphere) and range determination is achieved simply using time-of-flight techniques. MST radars generally rely on having a narrow beamwidth, so that lateral variations within a beam are not convolved with height variations. Typical range resolutions are of order 150 metres.

MST radars are found all over the world and vary considerably in design, from large atmospheric research radars to small wind profilers used, for example, to monitor atmospheric conditions close to airports. Some of the larger and more complex MST radars are sufficiently powerful that they can be used as incoherent scatter radars in their own right; examples are the MU radar in Japan and the EAR radar in Indonesia. For these systems, however, the performance for incoherent scatter is not optimal because their transmitters are not as powerful as those of dedicated ISRs.

Data from the NERC MST Radar Facility at Aberystwyth - <http://mst.nerc.ac.uk> Plotted 2009/03/09 09:50 UT  
 Source: 46.5 MHz MST Radar, 300 m range resolution, 30 minute averages, latest 24 hours

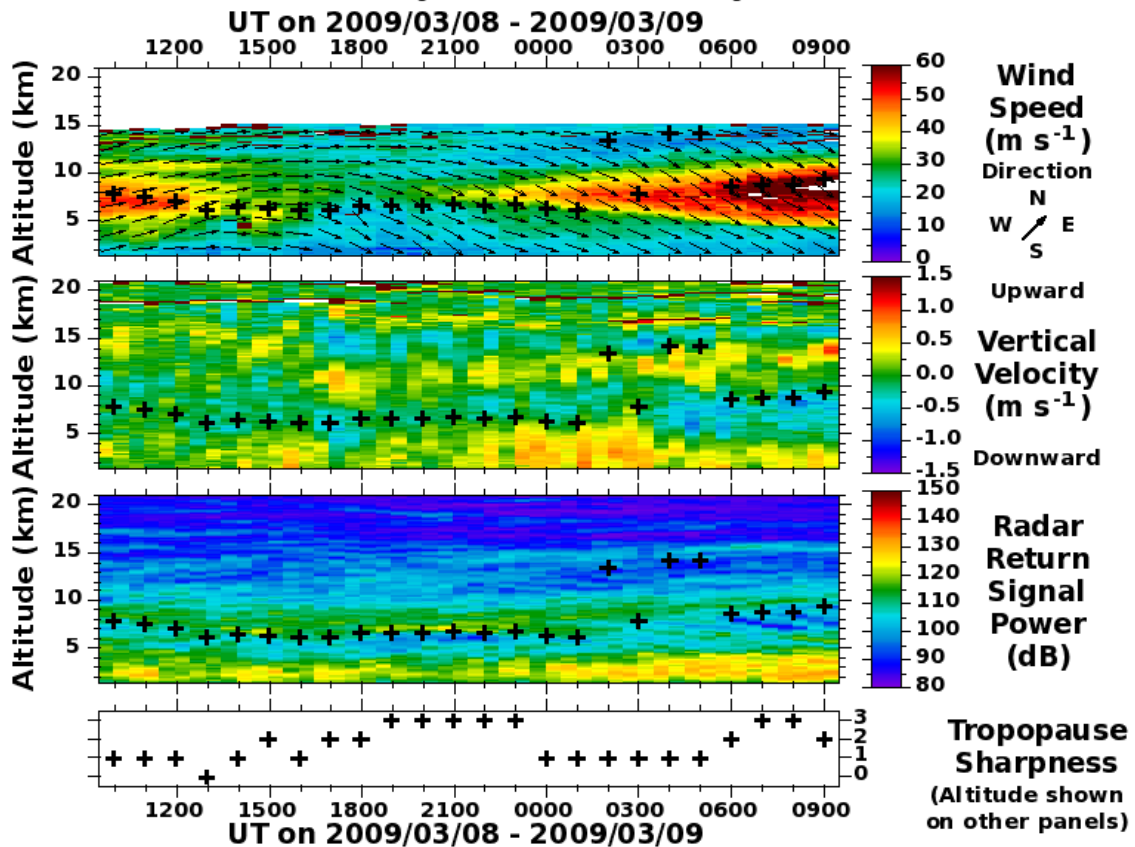


Figure 8: Typical daily stratosphere and troposphere data set from the Capel Dewi MST radar (from the NERC MST radar facility web site <http://mst.nerc.ac.uk/IMAGES/>)

A number of MST radars are already deployed in conjunction with incoherent scatter radars, and provide considerable synergy because they enable the lower atmosphere to be monitored at the same time as the ISR studies the behaviour of the upper atmosphere. On Svalbard, for example, the SOUSY radar (<http://radars.uit.no/sousy/index.html>) is a 53.5 MHz MST radar operating in close proximity to the ESR, using an array of 356 yagi antennas with an overall diameter of 95 metres. The total average power from the SOUSY system is around 200 W, very much lower than the power consumption of an incoherent scatter radar. At Tromsø, the MORRO radar is a 56 MHz MST radar, operated by the University of Tromsø, which consists of 144 four-element yagi antennas in a square array of side 50 metres. The total peak power is around 90 kW with a maximum duty cycle of 10%.

### 3.1.3. Meteor Scatter Radars

Meteor scatter radars are somewhat similar to MST radars, but are specifically designed to receive backscatter from the intense ionisation trails generated by the ablation of meteors as they burn up in the Earth's lower ionosphere, at altitudes between 80 and 100 km. Typical count rates for echo-producing meteors vary from around ten per hour in the evening to several hundred per hour near dawn. These radars are particularly suitable for the study of atmospheric dynamics in the

mesosphere and lower thermosphere, since the Doppler shift of the meteor echoes allows a determination of the neutral wind field in which the meteor ionisation is drifting. The time taken for the meteor ions to recombine also provides information on the temperature and chemistry in this region of the atmosphere. A key use of meteor scatter radars is to establish the climatology of waves and tides in the mesosphere and lower thermosphere, with statistical methods being used to obtain the properties of waves whose periods can be much longer than the mean time between the arrival of meteors. Measurements of the speed and direction of the incoming meteors are also important in their own right, in establishing the characteristics of the different meteoroid populations within the solar system.

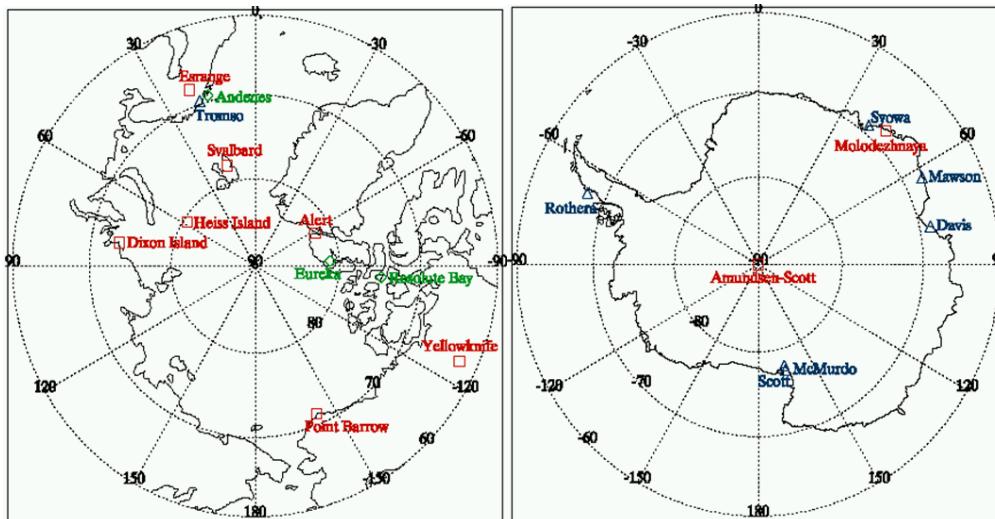


Figure 9: Current high-latitude coverage of MST and meteor scatter radars (source: Tony van Eyken).

Meteor radars are normally smaller and simpler systems than MST radars, though operating at similar frequencies, typically from 30 to 70 MHz. In their simplest form, meteor radars use receiving antennas only, relying on commercial broadcasters to provide the transmitted signal. At a slightly higher level of refinement, a very common type of meteor radar is the All-Sky Interferometric Meteor Radar (SKiYMET), which uses one transmitting antenna together with an array of five receiving antennas, arranged in a asymmetric cross and acting as an interferometer. The arms of the cross are around two wavelengths in length, and each receiving antenna is connected to a separate receiver system. Detection of meteor trails occurs when these are close to perpendicular to the meteor radar beam direction, and the different arrival times of the received signals at the receiver antennas allow direction information to be recovered. With such a small receiving array, it is not possible to recover radiants for individual meteors, although this can be done statistically. More sophisticated meteor radars have been constructed with multiple receiver arrays, and allow good orbital information to be established for individual meteors. Examples of such radars include the Advanced Meteor Orbit Radar (AMOR, Baggeley et al 1994) and the Canadian Meteor Orbit Radar (CMOR, Webster et al, 2004). Incoherent Scatter Radars are also used as meteor scatter radars, and in particular the tristatic EISCAT UHF system has the ability to make simultaneous observations of the same meteor from three different look directions, enabling orbital parameters to be

established. The same will be true of EISCAT-3D, given its multistatic capability for lower ionospheric observations.

Because there is considerable interest in establishing the geographical variation in the dynamics of the mesosphere and lower thermosphere, and in comparing the meteor flux seen at various latitudes, meteor scatter radars are found in a wide variety of locations worldwide. They are also often co-located with incoherent scatter radars, with examples including the Nippon/Norway Svalbard Meteor Radar close to the ESR, and the SKiYMET radar at Esrange in Sweden, which has conducted a number of common experiments with EISCAT.

#### 3.1.4. Partial Reflection and API experiments

Partial Reflection Experiments (PREs), also known as MF radars, are used to probe the structure of neutral winds in the altitude range from 60 to 90 km. A typical PRE uses vertical transmissions of frequencies around 2 MHz, which are Fresnel scattered by weakly solar ionised stratified layers and irregularities in refractive index in the ionospheric D-region. The backscattered signals give rise to a diffraction pattern on the ground, which is sampled by multiple receivers. A technique known as Full Correlation Analysis (FCA) is then used to extract wind information from these data, and can be used to obtain both mean winds and gravity wave data with time resolutions of order 2 minutes. Particularly at night time, when ionospheric critical frequencies are low, MF radar signals can penetrate far into the meteor scatter region, where they can also be used for studies of meteor echoes as described above. A further application of PREs is the study of Isolated Lower Mesosphere Echoes (ILMEs) which occur during periods of enhanced D-region ionisation due to Solar Proton Events, and have been identified as being related to the same low-altitude turbulent phenomena which give rise to Polar Mesosphere Winter Echoes seen, for example, by the EISCAT VHF radar.

Partial Reflection Experiments tend to be similar in design to the simpler meteor scatter radars, with a single transmitting antenna and a small number of spaced receivers. The transmission is generally pulsed, with pulse lengths of tens of microseconds and an inter-pulse period of some tens of milliseconds, giving a height resolution of order 5 km. As with MST and meteor scatter radars, a number of PRE systems exist at various locations around the world, including one at Tromsø (no longer operational) which has been operated as a collaboration between the University of Tromsø and the University of Saskatchewan, Canada. The Tromsø Dynasonde (see section 3.2.1) can also be used as a Partial Reflection Experiment, utilising its so-called "P-mode".

A refinement of the partial reflection technique is the creation of Artificial Periodic Irregularities (APIs) to provide man-made scattering targets for MF probing, rather than relying on the presence of naturally occurring irregularities. The API technique can significantly extend the altitude range over which partial reflection techniques can be used for atmospheric sounding, as well as being able to increase the amount of time during which such techniques can be used. In API experiments, a powerful HF transmitter, such as that used in the HF Heater at Tromsø, is used to produce a standing wave pattern when the HF signal is reflected from the ionospheric F region. The standing wave is created by the interaction of the transmitted and reflected HF

signals, and gives rise to electron density irregularities on the order of one part in a million, which can occur down to altitudes as low as 50 km. A PRE is then used to scatter from these irregularities. By measuring the period of the API oscillations, it is possible to estimate the ion-acoustic frequency and hence infer information about the plasma temperature. API experiments have been successfully performed at EISCAT using the HF Heater, Dynasonde and PRE, and the results have been compared with incoherent scatter radar measurements, showing reasonable consistency.

#### 3.1.5. Magnetospheric Radars

In addition to the radar modes described above, a few speculative attempts have been made to detect backscatter from structures in the Earth's magnetosphere at ranges from 1000 to 8000 km. This requires pulsed operations using a very high power HF transmitter system such as an ionospheric heater. In this mode of operation, the aim is to avoid any interaction with the ionosphere, so the sounding frequency should be higher than the ionospheric critical frequency, and high powers are used to maximise the detectability of the backscatter. Very long inter-pulse periods are used so that there is no range ambiguity which might result in ionospheric echoes being confused with returns from the magnetosphere.

### **3.2 Ionospheric Sounders**

HF sounding of the ionosphere is a very old technique, dating back to the first experiments which discovered the existence of the ionosphere. In contrast to the partial reflection technique described above, HF sounding relies on the total reflection of the incident sounding wave by the ionosphere, which occurs at frequencies up to 30 MHz. At these frequencies, the incident sounding wave is strongly refracted as it passes through the ionosphere, and experiences total reflection at the altitude where the ionospheric plasma frequency equates to the frequency of the sounding wave. Because of this, different sounding frequencies are reflected from different heights, up to the peak altitude of the F2 layer. Sounding frequencies above the F-layer critical frequency are not reflected, and such signals are lost into space. Because the technique relies on total reflection of the incident signal, it cannot be used to probe the structure of the ionosphere above the F-region peak, nor can it be used to probe the structure of electron density "valleys", local minima in the altitude profile of electron density, such as those which occur between the E and F regions of the ionosphere. The shape of the electron density profile from these regions is therefore generally modelled on the basis of the results from those parts of the density profile which can be observed.

The ionospheric plasma is also birefringent at HF frequencies, so that signals which have left-hand and right-hand polarisations with respect to the magnetic field direction follow different propagation paths. Thus a typical HF sounding transmission splits into two received signals corresponding to the above polarisations, known as O and X modes respectively.

#### 3.2.1 Ionosondes

Ionosondes generally employ swept-frequency transmitters, which scan through the full range of possible HF reflection frequencies, transmitting narrow pulses in the

vertical direction, and measuring the echo delay time as a function of frequency. Multiplying the delay time by the speed of light yields the so-called "virtual height" for the layer which reflects each sounding frequency; the true height profile is then obtained by using standard modelling techniques to invert the virtual height profile. Although they have very limited capabilities compared to instruments such as ISR, the cheapness of ionosondes allows them to be deployed in wide-scale networks, so that they have become very standard tools for ionospheric monitoring. The shape of the echo traces not only allows the density profile of the ionosphere to be determined, but also allows the presence or absence of structure to be determined through the existence, for instance, of features such as spread-F and sporadic-E. Modern ionosondes are, however, able to do much more than simply measuring density profiles. For example, the use of multiple spaced receivers allows the spatial distribution of ionospheric density irregularities to be calculated and presented as skymaps. The measurement of phase from irregularities in different directions allows estimates of the plasma velocity to be calculated.

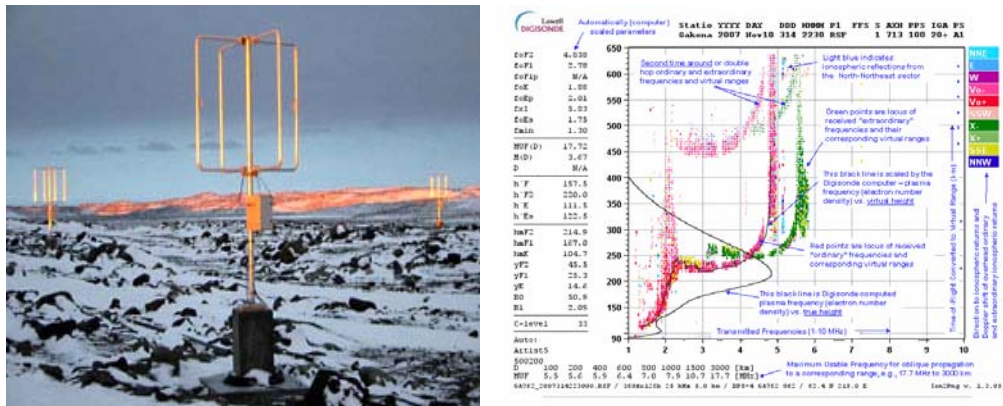
Because of their relative cheapness, and because they provide an independent measurement of the ionospheric profile which is not strongly dependent on instrument calibration issues, ionosondes are frequently deployed alongside incoherent scatter radars, where they provide important complementary measurements. Below we briefly review the two main types of ionosondes currently used by the ionospheric research community.

The digisonde (e.g. Reinisch, 1996) is the most popular type of commercially-produced ionosonde, comprising a low power, wide bandwidth transmitter, a single transmitting antenna and four distributed dipole receivers. The system is optimised for simple real-time monitoring of ionospheric critical frequencies for communications purposes. The following seven parameters are measured simultaneously.

- frequency
- range (equivalent to height for vertical incidence)
- amplitude
- phase
- Doppler shift and Doppler spread
- angle of arrival
- wave polarisation

The digisonde has the ability to optimise its use of transmitter power by not only applying coherent integration (the use of multiple successive phase coherent pulses) but also so-called spectral integration, in which the phase relationship of successive pulses is matched to trends in the ionosphere, such as Doppler shifts. This allows the coherent integration of successive pulses over any period during which the returned phase varies linearly. Digisondes also employ pulse compression using

complementary code sequences as a way of maximising their returned signal and thus avoiding the need for a high-power transmitter.



Figures 10 and 11: Digisonde receiving antennas at Davis station, Antarctica, and a typical ionogram from the Digisonde deployed in conjunction with HAARP, Alaska.

Although quite sophisticated data products can in principle be derived from Digisonde measurements, these are not available from many of the systems deployed around the world, and many users such as the US Air Force run Digisondes as survey instruments to provide real-time monitoring of a few ionospheric prime parameters.

The Dynasonde (e.g. Wright and Pitteway, 1979a,b) is another form of advanced ionosonde, specifically developed for the study of ionospheric dynamics. Like the Digisonde, Dynasondes cover the full sounding range from less than 1 MHz up to 30 MHz. Unlike digisondes, however, they utilise transmissions consisting of multiple pulses on a number of different frequencies, with the frequency offsets being of order 1 kHz. Complex algorithms are then used to discriminate between ionospherically reflected Dynasonde signals and external interferers such as communications users and commercial broadcasters. The main difference between the Digisonde and Dynasonde concepts lies in the detection software used to identify the echoes. Rather than using FFT techniques, the Dynasonde uses the consistency of time of arrival between the various sub-pulses as a means of identifying real echoes and distinguishing them from spurious interfering signals. Also, in contrast to the Digisonde, the Dynasonde software has tended to be more open to interaction from the user community, meaning that it has tended to be regarded as a better research tool, whereas the digisonde is more of a network/monitoring instrument.

### 3.2.2. HF Doppler Systems

HF Doppler systems are generally based on simple HF transmitters, ideally capable of multiple simultaneous frequencies, and a network of widely spaced receivers (baselines of tens to hundreds of km). An HF Doppler system is used to investigate the propagation of acoustic gravity waves in the upper atmosphere. These waves manifest themselves as Travelling Ionospheric Disturbances, which shift the isocontours of electron density up and down as the wave train passes through the reflection point of the sounding signal. This movement produces a change in phase path, and a Doppler shift proportional to the rate at which the phase path is changing. By monitoring three or more propagation paths, it is possible to measure the time at

which a given wave signature arrives at the different reflection points, and thus measure the speed and direction of the wave by triangulation. The resulting TID velocities provide an accurate representation of the horizontal and vertical velocities of the underlying wave. The use of multiple frequencies allows the wave properties to be measured at different heights, though the system is most sensitive to fluctuations at frequencies reflected close to the F-layer peak. Although the same analysis can be done from ionosonde data, and from TEC measurements, HF Doppler systems offer a very direct way of measuring wave parameters. They are also very cheap, with many systems using simple commercial receivers and making use of commercial HF broadcasters to provide the reference transmissions.

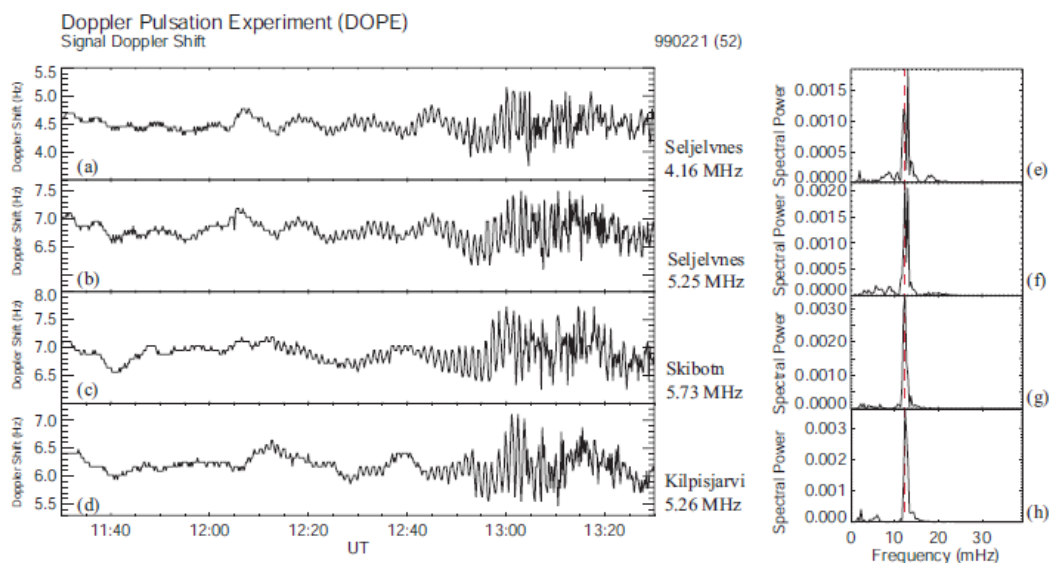


Figure 12: HF Doppler traces from the DOPE experiment, operated at EISCAT, showing gravity wave and pulsation activity, together with pulsation spectra (from Baddeley et al, 2005).

### 3.2.3. Oblique sounders

Oblique sounders use much the same hardware as the ionosonde instruments discussed in 3.2.1. The only difference is that, whereas ionosondes usually transmit vertically with a co-located transmitter and receiver, oblique sounders transmit at an oblique angle, with a separation between the transmitter and receiver which can be hundreds or even thousands of kilometres. The usual application of oblique sounders is to determine frequency management strategies on given communications links, or for the improvement of propagation models or communications channel simulations. Oblique sounders also provide an excellent opportunity to verify the predictions of ray-tracing codes and other propagation tools. Because they combine spatial and altitude information, the ionograms produced by oblique sounders are generally more difficult to interpret than those from vertical sounding, and they are often prone to multi-hop and multi-path effects. However, oblique sounders are often the only possible tools to monitor the state of the ionosphere above inaccessible regions such as oceans, for which vertical sounding is not practical. It should also be noted that the range of frequencies which can be used for oblique propagation is significantly larger than that which is used for vertical incidence sounding, because the ionospheric critical

frequency should be multiplied by a factor  $\sec(\phi)$ , where  $\phi$  is the angle between the sounding signal and the vertical.

### 3.3 LIDARS

Lidars are in many ways the optical analogue of radars, since pulses of laser light are used as the sounding signal, which is scattered from structures in the atmosphere. As with radars, the range to the target is determined by simple time-of-flight arguments, and the instrument is only sensitive to objects whose scale size is the same as the sounding wavelength or longer. Lidars are a standard tool in sounding the lower atmosphere, using frequencies in the ultra-violet, visible or near infra-red. Pumped dye lasers are used to produce the sounding signal, with etalons being used to compress the line-width of the emitted laser beam and collimators being used to control its angular spread. Pulse lengths vary from a few nanoseconds, up to almost a microsecond. Detection is done by optical telescopes, linked to photon-counting electronics such as photomultiplier tubes (PMTs) or Avalanche Photodiodes (APDs). The scattering targets are provided by effects such as aerosols and cloud particles, though any feature which produces a dielectric discontinuity will in principle give rise to a scattering effect.

Lidars, like radars, have the advantage of very high resolution compared to other types of instrument. Over time, a substantial body of work has been dedicated to extracting atmospheric parameters such as temperature, pressure, humidity, wind speed, composition, particle properties, cloud density and structure. As with radars, the more advanced lidars can be scanned, and complex optical configurations are sometimes used to make possible fast scanning or wide angular coverage. The difficulty is that the more advanced lidars are very complex instruments, unsuited to unattended operation. However there are also a range of simpler, more robust lidars which can be used at remote sites. Most atmospheric lidars are aimed at the study of the lower atmosphere and are powerful observing tools in meteorology. Usable wavelengths for lidar studies fall in the range 250 nm to 1.1 micrometres, though the scattering mechanism is different depending on the wavelength used.

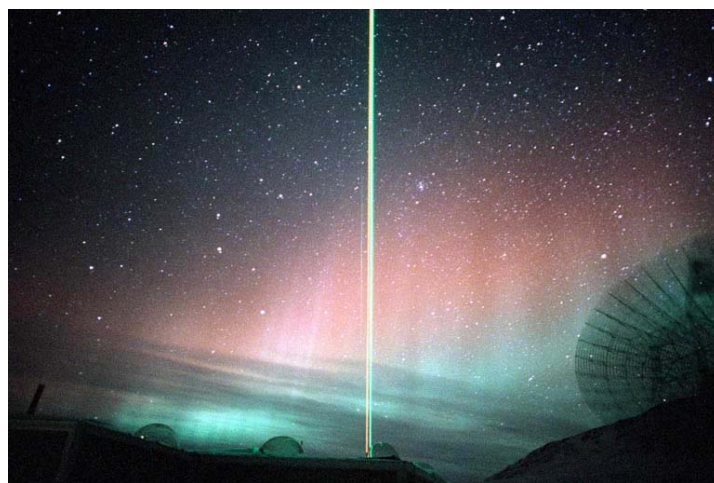


*Figure 13: The ARCLITE lidar facility at the Sondre Stromfjord ISR site(source Sondrestrom web site).*

Rayleigh lidars can probe the neutral density between altitudes of 45 and 90km under nighttime conditions. This technique relies on Rayleigh scattering, the scattering of radiation from atmospheric molecules. This type of lidar therefore provides an excellent tool for measuring atmospheric density. Rayleigh lidars can also exploit Mie scattering to probe the concentration of atmospheric aerosols, though generally in a lower altitude range, of perhaps 3 to 30 km. Approximations to Mie scattering can also be used to describe scatter from ice crystals, atmospheric dust, sea-salt particles etc. Lasers such as the Nd-YAG laser are used to produce the sounding signal, with the second harmonic (532nm) being a popular wavelength for this kind of study. A typical average power is of order 10 Watts per beam, with telescope apertures in the range 1 to 2 metres. Advanced lidars typically employ more than one beam, and have some capabilities for frequency agility. Because of the strength of Rayleigh scattering of solar radiation during the day, the use of such lidars is essentially confined to nighttime conditions.

Raman lidars make use of an inelastic scattering process in which the incident radiation changes the vibrational-rotational energy level of the atmospheric molecules. This produces a frequency shift in the scattered radiation which corresponds to the difference between the initial and final energy states, which in turn depends on the molecule under test. Because of these properties, results from Raman lidars can be used to calculate both atmospheric temperature and composition, however the cross-section of Raman scattering is low, and hence the technique is limited to particularly abundant atmospheric species such as water vapour.

A standard technique in atmospheric lidar sounding is known as DIAL (Differential Absorption Lidar) in which two sounding wavelengths are used, with one being absorbed more strongly than the other. Knowing the differential cross-section between the two wavelengths, it is possible to make quite sensitive measurements of atmospheric composition using the DIAL technique. DIAL can be used with both Rayleigh and Raman scattering, and has become a standard technique for measuring the abundance of certain atmospheric constituents, such as water vapour and ozone.

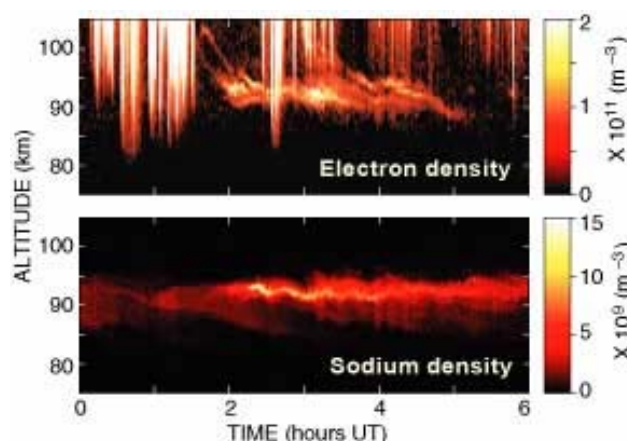


*Figure 14: E-region electron density enhancements measured by the Sondrestromfjord radar compared with sodium enhancements observed by the ARCLITE lidar (source Sondrestrom web site).*

Sodium lidars, with a wavelength around 589 nm, make use of resonance fluorescence scattering, which is much stronger than Rayleigh scattering. These lidars can measure all the way up to the central E-region, around 110 km, where they can scatter from sodium layers produced by meteor ablation or rocket launches. Sodium lidars can measure temperatures and winds, as well as being able to recover gravity wave fluxes from the mesopause region. This kind of scattering is strong enough to be used during daylight, although filters have to be used to recover the sodium fluorescence signal, and long integration times cannot be avoided unless these filters are very specialised. For upper atmosphere measurements, however, the required integration times are fairly long, typical values being 5 minutes for night-time observations and 25 minutes during daytime. Characteristic errors are therefore also significantly larger during the day.

### **3.4 Passive Optical Imagers**

The most prevalent optical techniques in solar-terrestrial physics rely not on sounding the atmosphere with lidar pulses, but on the passive observation of naturally-produced optical emissions, which arise over a broad range of frequencies. Of course the best-known of these natural optical emissions are those which are produced in the aurora, through the decay of excited states produced in the interaction of atmospheric species either with primary precipitating ions and electrons, or with the secondary ionisation which these primary particles produce when they enter the neutral atmosphere. As well as the aurora, which is confined to a relatively narrow geographical region, there is an ever-present weak natural emission known as airglow, arising from the decay of excitations produced either by sunlight, the combination of oxygen and nitrogen to form nitric oxide (in which a photon is released) or through other types of energy exchange. A detectable airglow flux can be seen anywhere on Earth during the hours of darkness, and airglow imaging is one of the most important techniques for measuring the behaviour of the neutral upper atmosphere.

#### **3.4.1. Auroral Imagers**

Most auroral imagers used in ground-based studies are essentially white-light cameras using a filter wheel with a number of optical filters. The filters serve to limit the sensitivity of the camera to a number of particular wavelengths in order to allow the form of the aurora to be imaged at a number of discrete emission wavelengths. These wavelengths correspond to various decay transitions whose occurrence is obviously sensitive to the energy of the incident ionisation and to the composition of the high-latitude atmosphere. Most of the observed auroral emissions originate from different transitions in nitrogen and oxygen, although a few arise from transitions in excited states of hydrogen and represent the collisions of incoming protons with species of the neutral atmosphere. As well as having different emission frequencies, the various excited states also have different lifetimes depending on a variety of quantum effects. This makes it possible to use certain emission wavelengths with short lifetimes (so-called prompt emissions) to study the high-resolution dynamics of precipitation at certain particle energies, while emissions with long lifetimes can only be used to study highly averaged temporal behaviour of auroral precipitation.

Some of the most common auroral emission wavelengths include 656.3 nm - the hydrogen alpha line, 636.4 and 630.0 nm - due to the decay of atomic oxygen,

557.7nm - also due to atomic oxygen, 486.1 nm - the hydrogen beta line, 427.8 nm - from  $N_2^+$ , and 391.4 nm, also due to  $N_2^+$ . While the excited state responsible for the 630 nm oxygen line can have a lifetime of more than 100 seconds, the excited states of  $N_2^+$  have lifetimes of less than a microsecond, illustrating how different wavelengths can be used to study the evolution of the aurora over different timescales. Because the atmospheric composition varies with height, the long-wavelength (red line) optical transitions of oxygen generally occur at F-region altitudes and correspond to low-energy precipitation, while the green and blue-line transitions of nitrogen represent more energetic particle precipitation and take place at lower F-region and E-region altitudes. The 557.7 nm green line transition in atomic oxygen is also characteristic of the E-region. Characteristic emissions in the aurora vary as a function of the time of day, which in turn reflects the variation in the acceleration process driving the particle precipitation. Around noon, the dominant precipitation is composed of low-energy particles entering the magnetosphere and ionosphere through the cusp, and therefore subject to only weak acceleration. Red line F-region emission is therefore dominant. Around magnetic midnight, however, the aurora is produced by precipitating particles which have been strongly accelerated in the magnetotail. Hence the night-time aurora tends to be dominated by the 557.7 nm E-region green line emission.

The objectives of auroral imagers are not exclusively to determine the characteristic energy of auroral precipitation - the main objective is to measure the structure and dynamics of auroral forms, which occur in a wide variety of different types, and to examine the relationship between variables such as structure, dynamics and energy spectrum to the driving processes in the Earth's space environment. The phenomenon generally referred to as an auroral arc is almost never a quiescent, homogeneous feature, but instead is invariably composed of a hierarchy of features, each having different scale sizes and dynamics, whose structures are closely related to underlying parameters such as the ionospheric electric field and field-aligned currents. These variables in turn relate back to the properties of the aurora, so that the aurora, ionosphere and magnetosphere represent a tightly coupled, highly non-linear system. Because of this complexity, auroral studies require a wide range of simultaneous observations, with high resolution in space, time and particle energy being desired. Indeed, the evidence shows that it is the accuracy of the available observations which still limits our ability to describe the aurora, since auroral structures are routinely seen on all spatial scales down to the highest resolutions currently available with optical imagers.

### 3.4.2 All Sky Imagers

Ground-based auroral instrumentation used for auroral studies has included television cameras, scanning photometers and CCD devices - but the all-sky imager (ASI) has been the mainstay of auroral physics for the last 50 years. These instruments measure the large-scale structure of the aurora, rather than the small-scale dynamics of particular auroral regions. All-sky imagers tend to be deployed in networks, with overlap between their viewing fields. A compelling recent example is the use of a network of 20 auroral imagers in the NORSTAR ASI array to image the large-scale properties of the aurora over the whole North American continent.

In general, an All-Sky Imager consists of a low-light-level television camera fitted

with a wide-angle lens. Narrow band filters at the primary auroral wavelengths can be used to study the large-scale behaviours of the principal auroral emissions. ASIs are generally operated entirely automatically, often in remote locations, with an onboard PC being used to calculate safe observing intervals in which the Sun and Moon do not wash out the auroral emission. Video images are generally averaged in time using a real-time frame grabber and image processing hardware. Automatic gain control is used to ensure that the captured images always have an appropriate dynamic range. Some form of flat-fielding correction is then performed to translate the image onto a geographic grid, where it is saved for later analysis. The data rate can be varied depending on the location of the instrument and the capacity of the available local storage. At one extreme, full all-sky videos can be recorded. At the other extreme data can be averaged for tens of seconds prior to storage of the integrated image. In the case of the NORSTAR ASI array, the default post-integration time is six seconds.



*Figure 15: A typical all-sky auroral image (from “An aurora watcher’s guide” by Robert C. Eather)*

### 3.4.3 High resolution auroral imagers

In contrast to All-Sky Imagers, high-resolution auroral imagers are addressing different physical problems. Rather than looking at the global-scale response of the auroral oval to drivers in the Earth's space environment, high-resolution imagers are focused on studying the small-scale physics of the aurora, whose behaviour is in general even less well-known. High-resolution imagers are not normally deployed in networks, but rather located at specific sites to support other high-precision instruments including incoherent scatter radars. The behaviours studied include

phenomena such as auroral fine structure (e.g. kinks and curls), flickering, multiple arcs, black aurora, thin arcs and auroral vortices. Because the aim is to interpret the causes and effects of these phenomena and their relationship to variations in other parameters, good supporting information from other diagnostics is a key requirement.

High-resolution imagers generally consist of a powerful primary telescope with a relatively small field-of-view, sometimes co-mounted with a less powerful secondary telescope whose wider view field provides contextual information, including a star field for calibration and verification of pointing direction. Both the primary and secondary telescopes are connected to image capture devices, normally CCD cameras linked to high-capacity digital video recorders. For both imagers, automatic gain control is needed in order to cope with the large variation in the brightness of the aurora, which can change by orders of magnitude on sub-second timescales. A GPS receiver is included in the imager set up to provide accurate timing information.

As discussed earlier, it is really desirable to measure the same volume of aurora simultaneously at multiple emission wavelengths in order to probe the variation of the aurora at different characteristic precipitation energies. Since the small-scale structure of the aurora also tends to be fast-changing, the use of a rotating filter wheel is less likely to be a suitable option than in the case of an ASI; hence the most advanced high-resolution imagers consist of multiple telescopes, each observing simultaneously at a different wavelength. Because of this, the volume of data from this type of instrument can become very large.

#### 3.4.4. Airglow Imagers

Airglow imagers share many of the properties of the auroral All-Sky Imagers discussed above. However, because airglow is seen throughout the world, airglow imagers are distributed globally, rather than just being confined to the auroral zones. Airglow principally occurs as a result of the excitation of the 1D meta-stable state of atomic oxygen, which radiates at 630 nm, and is also present in the aurora. Unlike aurora, however, airglow emissions are much less structured and very weak so that they are normally sub-visual.

Because airglow is very faint compared to auroral emission, the requirement in these instruments is for sensitive cooled detectors, so that thermo-electronically cooled CCDs are often used to provide a very low noise environment. Airglow can occur at a number of characteristic wavelengths so that, as with ASIs, filter wheels are often used in conjunction with airglow imagers to cycle between the different wavelengths being imaged. In some advanced systems, multiple imagers with different filters are used to make simultaneous observations. As with the ASI, the airglow imager employs a wide angle lens, so that a subsequent flat-field correction has to be applied. The sensitivity of the instrument makes it extremely important that daylight or any other bright light should be excluded from the sensor, so that these instruments normally employ some kind of computerised detection system to control the opening of the shutter.

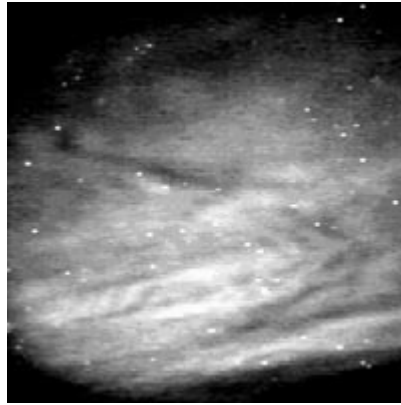


*Figure 16: An intensified airglow image, showing signatures of gravity wave activity (by Mike Taylor and Larry Gardner, Utah State University).*

The intensity of the airglow emission is used as a proxy for the electron density of the upper atmosphere, and so is used to probe density structures caused by processes such as atmospheric waves, and to test the validity of atmospheric models. Measuring the line width can provide information about the neutral temperature, while the Doppler shift of the emission line is also used to measure the neutral velocity, in instruments such as the Fabry-Perot Interferometer (see below). At EISCAT, airglow imagers have also been used in conjunction with ionospheric modification (heating) experiments, to study the flux of high energy electrons caused by wave-particle coupling processes, which in turn cause energisation of atomic oxygen in the neutral atmosphere, producing so-called "artificial aurora".

#### 3.4.5. Fabry-Perot Interferometers

A particularly specialised optical instrument for studies of auroral and airglow emissions is the Fabry-Perot interferometer, which typically consists of either a glass plate with two highly reflecting surfaces, or two highly parallel spaced reflecting mirrors, known as an etalon. The transmission spectrum of the instrument exhibits a number of peaks, corresponding to resonances of the etalon, the variations in transmission function being caused by the multiple reflections of light between the two reflecting surfaces. If the interfering beams are in phase, the result is constructive interference and a high transmission function, but if they are out of phase the result is destructive interference and low transmission. The phase relationship of the beams depends on the wavelength of the incident light, the angle at which it travels through the etalon, the etalon thickness and the refractive index of the material between the two reflecting surfaces. The etalon therefore acts as a dichroic filter, with sharp peaks in transmission and broad frequency regions in which no signal is transmitted. The sensitivity and spectral resolution of the device are very good, which explains why this instrument is so highly favoured for optical studies in geophysics, because the emissions being studied are faint and the Doppler shifts of the emission lines are typically very small.

While early FPIs observed only a single patch of sky, more advanced modern systems such as the Scanning Doppler Imager (SCANDI) (e.g. Conde and Smith, 1995) use a fish-eye lens and a rotating mirror, at an elevation angle of 30 or 45 degrees, allowing them to measure light from different directions over a very wide area. The light from

the mirror passes through an etalon, a focusing telescope and an interference filter, before being sensed by a detector, which in modern systems is generally some kind of cooled CCD.

The resulting observation consists of a series of concentric interference rings, whose width is partly due to the temperature of the emitting gas, and so can be used to derive the neutral temperature. If the gas is moving, the rings will move inward towards the centre of the pattern if the gas is moving away (red shift) or outwards in the case of a motion toward the observer (blue shift). By measuring the component of the wind in several lines of sight, a wind vector can be computed. Because the elevation angle of the observation is relatively low, and the emissions come from F-region altitudes, the regions measured by FPIs are several hundred kilometres from the instrument itself, allowing the neutral velocity field to be mapped over an area of several hundred km. For this reason, FPIs (like auroral imagers) are best deployed in widely spaced networks. In northern Scandinavia, three FPIs at Ramfjord (Tromsø), ESRANGE (Kiruna) and Sodankylä have been used to make direct tristatic observations of neutral vector velocity.

The most usual imaging wavelength for an FPI is the 630nm oxygen line, but an additional line of great interest is the 832 nm hydroxyl emission line, which originates at low altitudes and so can be used to study the temperature and dynamics of the mesosphere.

#### 3.4.6 Photometers

A photometer is any instrument used to measure irradiance, and such instruments have a broad range of applications in space science to study light intensity and absorption. In their simplest form, photometers consist of photoresistors or photodiodes whose varying electrical properties can be measured by suitable electronics. For low light level applications, photometers can use photon-counting electronics as their detection mechanism.

Photometry is a standard technique for studying both auroral emissions, using various wavelengths to probe the variation of auroral forms at the characteristic emission frequencies, because comparisons of intensity at these frequencies can be used to make estimates of the characteristic energy flux of the auroral precipitation. They have also been used on both satellites and sounding rockets to make in-situ observations of the variation in auroral emission rates as a function of altitude. For auroral work, photometers normally employ narrow-band filters and photomultiplying electronics.

Ground-based auroral photometers are used in two standard configurations; field-aligned or scanning. In field-aligned mode, the photometer is oriented parallel to the magnetic field, and observations are a simple time series of emission intensities.

Meridian Scanning Photometers (or MSPs) use a moving mirror, which scans back and forth across the sky in the magnetic meridian to get a broader view of the variation and motion of auroral forms. Interpretation of the results is straightforward in the case of slowly-moving aurora, but can be complex for rapidly-varying aurora whose form and position change on timescales quicker than the scan time of the

mirror. Geometric corrections also have to be applied in order to derive true variations in position from the data measured by the instrument

#### 3.4.7 Radiometers

Irradiance can also be measured using a radiometer, in which the incident radiation is absorbed by a bolometer, raising its temperature. Several different types of radiometers exist, some using direct measurements of the bolometer temperature in comparison to hot and cold reference bodies, others using vanes which begin to spin when exposed to radiation of the correct wavelength. In atmospheric physics, microwave radiometers, combining a microwave receiver and a spectrometer, are used to study the rotational transitions of various atmospheric trace gases, including ozone and water vapour. Although these gases are concentrated at sub-ionospheric altitudes, monitoring their concentrations can shed light on the effects of upper atmospheric processes, such as energetic particles, on the middle and lower atmosphere. The profile of trace chemical composition can be derived from the shape of the pressure-broadened transmission line. Because the atmospheric signal is normally weak, advanced techniques must be used to enhance the signal for subsequent detection. Downconversion of the incident signal is used, as in radars, meaning that radiometers are often complicated systems.

#### 3.4.8 Spectrometers

Spectrometers are also widely used in auroral studies for simultaneous multi-wavelength imaging. In a standard auroral spectrometer, the auroral image is focused onto a diffraction grating, and the resulting image is then projected onto a cooled CCD array. By varying the spacing of the grating, the wavelength sampled by the spectrometer varies, and spectrometers commonly employ some mechanical method such as tilting the grating, or using a filter wheel, which enables the instrument to scan in frequency. The resulting image retains some information about auroral spatial variations in the direction of the entrance slit which lets in the incident light. The advantage compared to other techniques is the ability to record the whole spectrum of integrated auroral emissions.

In more advanced spectrometers, the diffraction grating is mounted on a prism which disperses the light spectrally and avoids the need to scan the grating. This provides much higher time resolution, which is essential since several types of auroral emission are highly dynamic. However, even for these instruments, integration times are of order of a few seconds, so that a combination of spectrometer and all-sky imager data is often needed to distinguish the effects of energy changes from those of arc motions. Integration times obviously depend on auroral intensity, but sub-second integration times have been used for spectral imaging of the brightest aurora by some spectrometers.

### **3.5 Passive Radio Instruments**

Earlier in this document, we looked at a number of active radio instruments, such as radars and ionospheric sounders, used for monitoring the solar-terrestrial environment. In addition, there is an important class of instruments which relies on

passive radio reception, including two very standard instruments which we review below.

### 3.5.1 GPS and Beacon Satellite Receivers

Passive receivers tuned to beacon satellite signals are an extremely powerful method of measuring the total electron content of the upper atmosphere and near-Earth magnetosphere. Beacon satellites transmit signals at one or more precisely known frequencies, which encode details of their transmission time. Measuring this signal with a ground-based receiver, allows an observer to determine the time taken between the transmission and reception of the signal. If the positions of the satellite and of the receiver are known, the delay can be compared to that expected based on propagation at the speed of light, and the delays imposed by the Earth's atmosphere can be determined. Early beacon satellite experiments used single satellites in well-known orbits. From 1978 onwards, however, when the first satellites of the GPS network were launched, beacon satellites have played a crucial role in worldwide surveying and position finding.

The current GPS system comprises a constellation of between 24 and 32 satellites, each transmitting two precise frequencies known as L1 (1575.42 MHz) and L2 (1227.60 MHz). From each of the visible GPS satellites, a pseudo-range is computed by measuring the travel times of signals from the transmitter to a given receiver. In principle, a minimum of three visible satellites is required to calculate a position by triangulation global positioning applications, but in practical applications signals from four satellites are used in order to provide an independent verification of the positional information.

Delays on the GPS signal are, however, imposed by both the ionosphere and the troposphere. The ionospheric delay depends on the frequency of the signal and the integrated electron density (total electron content) along the slant path from the receiver to the spacecraft. The tropospheric delay depends on the integrated water vapour content along the slant path, but does not depend on frequency. Advanced receivers use the dispersive behaviour of the plasma to calculate the ionospheric correction, by measuring the differences in the delay between the two transmitted frequencies and using this to derive an estimate of the TEC.

Dual frequency GPS receivers are widely available on the commercial market, selling for a few hundred Euros. Such receivers are normally deployed in geographic networks, and, at least in the developed world, these are closely spaced. Because of this, large numbers of slant path estimates of TEC are available simultaneously, and these can be used as inputs to a mathematical inversion, in order to resolve the three-dimensional distribution of the electron density in the Earth's plasma environment. This kind of GPS tomography requires some assumptions, such as underlying basis functions to constrain the allowed variability – but in principle it allows the complete mapping of the time-dependent ionosphere, with Kalman filtering techniques being used to help determine temporal variability. Independent calibration information, e.g. from an ionospheric sounder, is also crucial in deriving the final electron density maps. The various constraints are now well-known, and well-developed techniques are used to address them, making GPS tomography a very powerful accompaniment to other kinds of monitoring in solar-terrestrial physics.

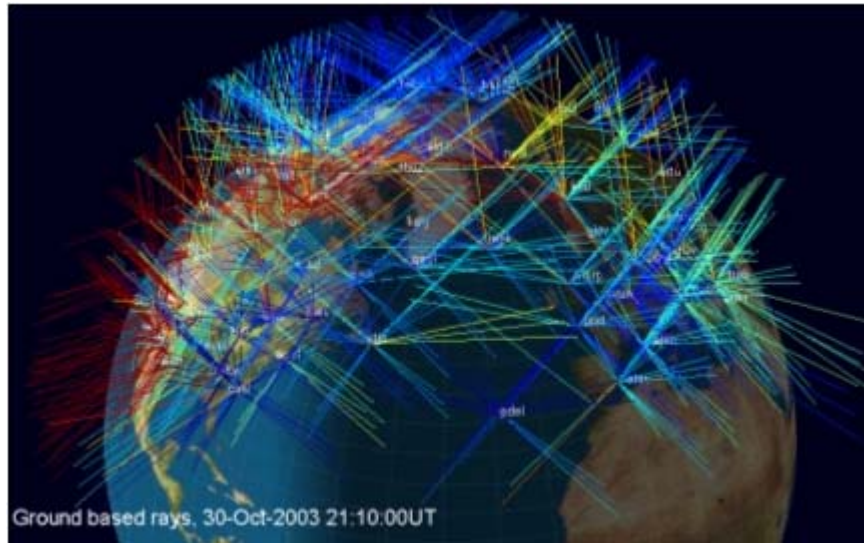


Figure 17: Depiction of GPS ray-paths used for tomographic imaging in the “Halloween Storm” events of October 30 2003 (source: University of Bath).

### 3.5.2 Riometers

A further standard passive radio technique for ionospheric studies is riometry, in which the intensity of cosmic radio noise, mainly originating from our own galaxy, is continuously measured from the ground. Riometers are based on the principle that, providing there is no absorption of the signals in the ionosphere, the pattern of cosmic radio noise repeats every sidereal day. Hence the technique consists of comparing each day’s measurements with an ideal “quiet day curve”, representing the signal intensity that the instrument would receive on a day with no absorption.

Ionospheric absorption occurs when the electron density of the D-region becomes enhanced, increasing the electron collision frequency. Absorption can occur due to two processes: deviative absorption, where incoming signals are subject to group retardation and refraction, and non-deviative absorption, in which the incoming signal loses its energy to the electrons of the lower ionosphere. The largest amount of absorption tends to occur at high latitudes, and is related to the auroral oval, but its occurrence is also greatly influenced by the occurrence of ionospheric storms. Sudden Ionospheric Disturbances can produce strong absorption enhancements for periods of 15-200 minutes after some types of solar events, while the most intense phenomena, known as polar cap absorption events, or PCAs, can cover the entire high-latitude region, and persist for a period of several days following a large solar flare. Because most absorption at riometer frequencies is associated with this kind of storm effects, riometers are a cheap method of investigating the effect of energetic particles on the Earth’s upper atmosphere, with strong implications for the effect on HF communications.

The most basic riometer consists of a single broad beam antenna, together with a self-calibrating radio receiver and some form of data acquisition system. The self-calibration is necessary in order to determine the intensity of the measured signal, by

regularly comparing it to that of a known stable calibration source. A range of frequencies can be used for riometry, typically between limits of 20 and 50 MHz.

In recent years, a new generation of imaging riometers has appeared, based on arrays of dipoles (typically 8x8 elements) forming multiple narrow beams, which can cover an area of more than 100 x 100km at 90km altitude. The IRIS, imaging riometer at Kilpisjarvi, Finland, for example, uses 49 beams with beamwidths of between 13 and 16°, scanned every second, with phasing achieved by a Butler matrix beam-forming network. This configuration allows the instrument to measure D-region absorption over a large area of northern Scandinavia.



*Figure 18: The IRIS imaging riometer at Kilpisjarvi, Finland (source: University of Lancaster).*

### 3.5.3 VLF and ELF receivers

A range of naturally-occurring radio emissions are found in the ELF and VLF regions of the radio spectrum, between frequencies of 0.3 and around 15 kHz. These include groundwaves from lightning strikes, ionospherically ducted radio signals from lightning, and long-duration whistlers which sweep downward in frequency from around 6 kHz to 0.5 kHz. The frequency range, and lower cutoff frequency of whistlers can be used to diagnose conditions in the magnetosphere, because the whistler waves are dispersively ducted along magnetospheric field lines. Some whistlers travel back and forth many times between the two hemispheres, creating very long wavetrains. So-called “nose whistlers” can be of very long duration, and can include both rising and falling frequency components.

During magnetically disturbed intervals, and particularly in the morning hours, the VLF range can be dominated by chorus, which consists of multiple superimposed signals, each of which rises monotonically in frequency. Chorus emission often occurs in chains of progressively rising frequency and is strongest at sub-auroral

latitudes, as chorus emission is related to the input of energetic particles into the Earth's upper atmosphere.

At Scandinavian latitudes, another frequent emission is “auroral hiss”, a broadband emission which, as its name implies, has no coherent evolution in frequency, though it sometimes resolves into dominant frequencies known as “wavering tones”. Hiss is directly related to the proximity of the aurora and is measured on the majority of days at auroral zone locations.

VLF and ELF emissions can be measured with relatively simple radio receiving equipment, linked to a spectrometer. These emissions are observed at a number of worldwide locations as a means of diagnosing the level of geomagnetic and auroral activity. Triangulation of lightning emissions is also carried out as a means of continuously mapping the global distribution of thunderstorms, which is important for both meteorology and studies of atmospheric electricity.

### **3.6 Magnetometers**

Magnetometry is one of the oldest and simplest techniques in geophysics. It consists of measuring the effect of solar-terrestrial processes on the Earth's magnetic field due, for example, to the currents induced in the ionosphere during auroral activity or perturbations in the magnetospheric ring currents. Magnetometers can also be used to measure much smaller variations in the Earth's magnetic field, such as magnetic micropulsations which occur when magnetic field lines oscillate at their natural resonant frequency due to energy release in the magnetosphere. The characteristic resonance frequencies are a function of field line length and electron density loading, so that ground-based magnetometers can actually be used to study the structure of the magnetosphere – a technique sometimes known as magnetoseismology.

Magnetometers are the classic network instrument, in that while results from a single magnetometer are often of limited use, the comparison of simultaneous magnetometer data from multiple locations allows the location and time history of magnetic disturbances to be determined. It also allows the change in field line resonant frequencies to be mapped as a function of location, which facilitates the mapping of magnetospheric structures as described above.

Within Europe, three magnetometer networks are currently operated. At high latitudes, the IMAGE network of magnetometers is located in Scandinavia and extending up to Svalbard. The Sub-Auroral Magnetometer Network (SAMNET) is mainly located in central Europe, though extends northward into southern Scandinavia. Finally the Southern Europe Geophysical Magnetometer Array (SEGMA) operates a range of stations in the south of Europe and around the Mediterranean. Comparable networks exist in North America, Greenland and East Asia. Most of the world's research magnetometers contribute their data to the global INTERMAGNET project, which acts as a global geomagnetic observatory.

#### **3.6.1. Fluxgate Magnetometers**

The standard type of research magnetometer is known as the “fluxgate” sensor, which comprises two parallel highly magnetic cores, each of which is wrapped by a primary

coil, but with the wrapping done in opposite directions on the two cores. Measurements are made by using a coil current to saturate the magnetic field in one of the cores. The first core to be magnetically saturated will be that in the direction parallel to the external field – the other core will have an induced field antiparallel to the external field, and will hence not reach saturation when the first coil is saturated. The difference between two cores induces a measured voltage in a secondary coil, and it is this voltage which is actually used to make the measurement. These instruments are stable over long periods of operation, relatively cheap to construct and accurate to tolerances of order 0.5 nT. They have therefore become the workhorses of the magnetometer community. One disadvantage of this type of magnetometer for certain uses is that the time resolution of the measurements is normally rather coarse (typically 10s for a basic fluxgate magnetometer).

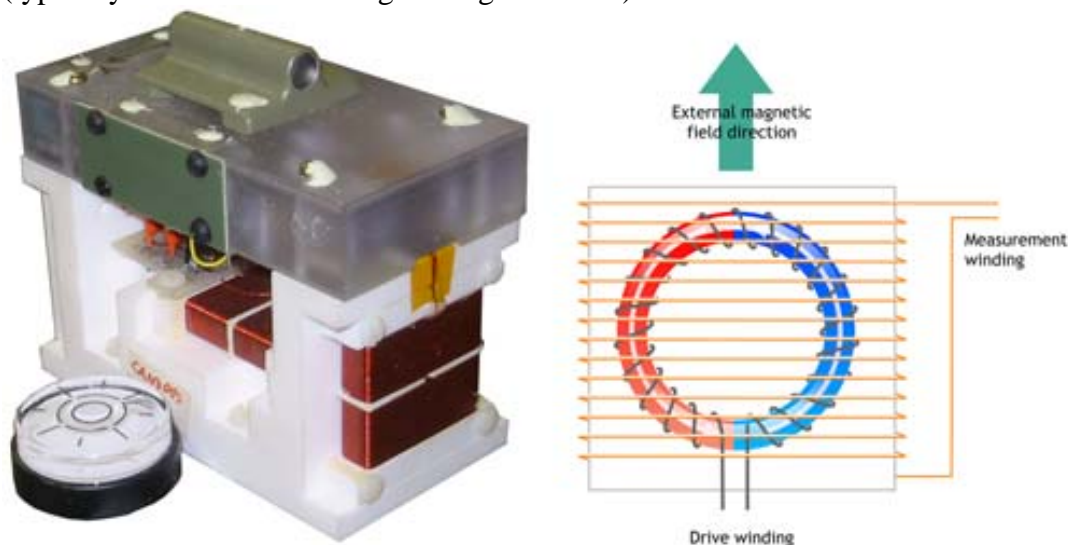


Figure 20: One of the fluxgate magnetometers used in the Canadian CARISMA array. The schematic on the right shows the arrangement of the core windings.

### 3.6.2 Proton Precession Magnetometers

This is a more accurate and more advanced type of magnetometer in which the protons of a proton-rich fluid are magnetised to align in the same direction and stop their normal precession. When released, they resume their precession in phase, inducing a voltage whose frequency depends on the ambient magnetic field. By measuring the frequency, the corresponding field is calculated.

### 3.6.3. Pulsation Magnetometers

A pulsation magnetometer typically consists of three search coils, a preamplifier and an A/D converter unit. Pulsation magnetometers differ from ordinary magnetometers in the fact that measurements of the magnetic field are made at much higher time resolution, and normally also with a much greater sensitivity. These systems, which typically sample at tens of Hz or faster, are designed to measure magnetic micropulsations in the frequency range from several milliHertz to several Hertz with accuracies of some tens of picoteslas.

### 3.7 Ionospheric Heaters

For completeness, we include one further important class of instrument used in ionospheric and magnetospheric studies, although it produces no data in its own right. Ionospheric heaters consist of HF transmitters which achieve a very high Effective Radiated Power (ERP) via a combination of high transmitter power and, usually more importantly, high antenna gain. Heaters exploit the fact that high-power electromagnetic waves transmitted into the ionosphere will heat the ionospheric electrons, causing modifications in the state of the plasma. When the transmitted frequencies of the heater coincide with natural resonant frequencies of the plasma, coupling can occur between the transmitted and natural modes, and such coupling may be non-linear, resulting in the growth and decay of ionospheric irregularities and the creation of plasma turbulence. Most heaters therefore use HF frequencies within the range of normal values for the ionospheric plasma frequency (i.e. 4 to 10 MHz).

Ionospheric heaters exist at many locations around the world, the most powerful being located at EISCAT (the Tromsø HF Heater), Sura (Russia), Kharkov (Ukraine) and HAARP (Alaska). Because heaters are essentially powerful transmitters, they do not record their own data, but rely on the presence of co-located radar systems of various kinds to diagnose the parameters to the modified ionosphere. Facilities such as EISCAT have had particular scientific success by using the Tromsø Heater with a combination of incoherent scatter radars and coherent scatter (CUTLASS) observations in the heated volume. Co-ordinated experiments have also been done by using the heater in conjunction with in-situ instruments mounted on satellites and rockets.

As stated above, heaters produce no data of their own, however these are flexible instruments, in which it is possible to vary parameters such as frequency, transmitter power, pulse length, beam direction and polarisation. It is often necessary to control these parameters to very high accuracy, making it important to preserve the necessary metadata relating to the heating operations in order to interpret the data from the associated diagnostics.



*Figure 21: The three antenna arrays of the EISCAT HF heating facility in Tromsø.*

#### **4. Existing facilities and Future Requirements**

In the previous section, we have made a comprehensive review of the possible types of observing instruments which might be deployed in association with EISCAT-3D. In the remainder of this report, we will address the question of the potential impact on the EISCAT-3D infrastructure, particularly on the data system, which would result if an appropriate number of such instruments were to be deployed at the EISCAT-3D sites – turning them, in effect, from radar sites into multi-instrument “STP observatories”. Before attempting to quantify this impact, however, we should examine the question of what instruments it would be appropriate to place at the various sites.

In its current design configuration, the EISCAT-3D system consists of a single large active site, and up to four passive receiver sites. The central site is envisaged as a permanently staffed site, housing not only the transmitters and the central receiver, but also the central archive and computing facility. It would be expected that there should also be provision for visiting scientists and experimenters, and that this site would be the scene of considerable experimental activity, including a variety of other instruments. The remote sites, however, are designed for long-period unattended activity on the basis that the remote sites will not be staffed, but that there will be automated control and monitoring and that error reporting and some fault-finding can be done remotely. Aside from regular maintenance visits, staff will only need to visit the sites when problems occur. If funding levels permitted, of course, more than one active site would be constructed, which would also imply the presence of staff at these locations, but in principle EISCAT-3D is always likely to consist of a mixture of active, staffed, sites and passive, unstaffed remote receivers.

This type of design implies some restrictions on the kinds of supporting instruments which can be placed at the remote sites. Instruments designed for long-period unattended operations would be an ideal complement to the remote arrays of EISCAT-3D, while complex instruments requiring regular operator intervention, such as sophisticated lidars, would not be good candidates to be placed at remote sites. Below, we briefly look at the classes of instruments mentioned in section 3, and summarise whether these would be useful instruments to deploy in association with EISCAT-3D.

##### **4.1 Other types of radars**

Coherent scatter radars tend to have large fields of view, each covering several degrees of latitude and longitude. In addition, because of the need to satisfy the orthogonality condition with the magnetic field in the observing volume, signals are transmitted and received obliquely, meaning that the volume of space above northern Scandinavia is best probed from radar sites in southern Scandinavia. The area above EISCAT is already covered by the two CUTLASS radars, located in Malvik (southern Norway) and Hankasalmi (southern Finland). Hence there would be no requirement to locate a coherent scatter radar in the vicinity of EISCAT-3D in order to undertake common volume observations. In recent years, however, there has been a substantial push by the coherent scatter radar community to cover polar, as opposed to auroral,

latitudes. This has led to the construction of the PolarDARN radar network, whose first radars were installed in northern Canada in 2007.

There is currently no PolarDARN radar in northern Europe, and preliminary discussions indicate that there would be potentially strong interest in siting a PolarDARN radar at one of the EISCAT-3D sites. However there is a preference for this to be at a passive EISCAT-3D site, to avoid any possibility of interference from the much more powerful EISCAT-3D system. This type of coherent radar is designed for long-period unattended operation, so locating it at an unmanned site would not be a problem. In this document, we have therefore studied the possibility of siting a coherent scatter radar on at least one of the EISCAT-3D remote sites.

In contrast to coherent scatter radars, meteor scatter and MST radars have smaller fields of view. However, an important part of the focus of these instruments is the study of wave modes such as tides and planetary waves, for which the wave number is quite small, i.e. the wavelength is long. For this kind of study, the optimal distribution is to have longitudinal chains of such radars, meaning that it would be redundant to have several radars in northern Scandinavia. There are already a number of MST and meteor scatter radars operating in this region, including the ESRAD and ALWIN radars at Andoya, the MORO radar at the Tromso EISCAT site and a SKYiMET meteor radar at ESRANGE. From the view point of large-scale neutral dynamics, there is probably no requirement for additional systems at the EISCAT-3D sites.

There may, however, be an argument for additional meteor or MST radars based on the study of smaller-scale dynamics. MST and meteor radars probe regions of the atmosphere which are heavily influenced by energy flowing upwards from below. These energy results are sensitive to the local topography, so that radars in the vicinity of mountains may obtain very different results to those located on plains. In principle, this means that there would be a good justification for deploying multiple middle atmosphere radars within the area covered by EISCAT-3D, especially if the different sites were located in significantly different terrain (i.e. on the windward and leeward sides of the Scandinavian mountain chain). From this viewpoint, we have included a study of the implications of locating a meteor scatter or MST radar at the central site, and at each of the two most distant remotes.

In the same way, there is a clear synergy in siting an ionospheric heater at the active site of EISCAT-3D, in order to conduct a wide variety of plasma physics experiments. Although the presence of an HF heater would have obvious implications for the amount of power and space required at the radar site, it would have no direct implications for the data rate, as the heater would produce no data of its own.

In summary, we recommend that each active radar site of EISCAT-3D should have sufficient infrastructure to accommodate either a meteor scatter or MST radar. There is likely to be a requirement to place a coherent scatter radar near to at least one of passive remote sites of EISCAT-3D, which would serve as a European contribution to the PolarDARN network. Likewise it might be desirable to deploy an MST or meteor radar at one or two of the EISCAT-3D remote sites to fill in gaps in the existing network coverage, but such a facility would not be necessary at each site.

## 4.2 Ionospheric Sounders

In principle, it would be useful to equip each site with a basic ionospheric sounder, in order to gain insight into the wider-scale structure of the ionosphere above the area covered by the EISCAT-3D arrays. The passive sites would not necessarily need a highly advanced sounder, but even if this were the case, the cost of the sounder would still be a fraction of that of the receiving array. The data from multiple sounders whose receivers scanned continuously through the HF band (even when the sounders were not transmitting) could probably be used fairly easily for HF Doppler analysis, based on the reception of commercial HF signals.

At the active site of EISCAT-3D, the presence of an ionospheric heater implies a compelling need for an advanced ionospheric sounder such as a Dynasonde. Among other things, this would allow the possibility to conduct studies of the lower atmosphere by the use of the API technique which could then be diagnosed by using the advanced sounder as an MF radar. Such a sounder would, in any case, be an essential complementary tool for calibration of the radar data in the event that no self-calibration could be done, e.g. by using the plasma lines.

During our discussions, a proposal has been made that two of our four remote sites should be kept as “radio quiet” sites, so that passive receiving equipment could be operated there without interference. If this proposal was adopted, the best strategy would probably be for the inner pair of remotes to be the quiet sites. Although no HF transmitter would be operated at these sites, HF receivers could still be sited there for passive radar and HF Doppler studies. The active site, and the outer pair of remote sites, should then be equipped with state-of-the-art HF sounders. At the central site, the sounder would be an essential accompaniment to the HF heating array and would be able to carry out calibration of the radar data if no other calibration was available. The sounders at the active remotes would provide valuable information about ionospheric structure above the radar network.

## 4.3 Active Optical Instruments (e.g. Lidars)

Studies of the coupling between the middle and lower atmosphere are a very high priority for the EISCAT-3D radars, so there should be a strong emphasis on complementary observing techniques for stratosphere, mesosphere and thermosphere studies. For any kind of comparative radar and optical study, genuine co-location of the facilities is an important requirement, because interpretation of off-axis optical data can be complicated, even if the baselines are relatively short. The requirement for co-located instruments generally becomes stronger as the altitude of the observation decreases. Having a co-located instrument such as a sodium lidar, capable of reaching stratospheric or even mesospheric altitudes, would be a very powerful complement to the EISCAT-3D radar, particularly under dark winter conditions. However, such instruments are complex and not well-suited to unattended operations, making them only really suitable for deployment on an active, staffed, radar site. More rugged lidars, better suited to remote operations, tend to have lower observing limits in altitude and, as such, there is not a compelling case to site such lidars at the remote sites of EISCAT-3D.

#### 4.4 Passive Optical Instruments

This category covers a broad array of instruments whose applications range through studies of auroral structure and dynamics, auroral spectroscopy, neutral atmospheric structure, neutral dynamics and atmospheric composition and chemistry. While some of these instruments are more complex than others, most of them are in principle designed for unattended operation and are intended to operate as part of a spatial network of similar observing instruments with overlapping fields of view. In the cases where similar instrument networks already exist, the baselines between instruments are of the same order as the prospective baselines between EISCAT-3D sites. Hence it would be logical to expect that each of the EISCAT-3D sites would be accompanied by an optical observatory containing a few such instruments.

As an example of the possible instrument complement of one such station, consider the current Canadian GeoSpace Monitoring (CGSM) network, which defines the current state of the art for networks of this kind. Several of the CGSM stations include an All-Sky Imager with a five-slot filter wheel and a Meridian Scanning Photometer. The All-Sky Imagers can measure at cadences up to 0.1 Hz, though the typical time resolution of the images is 20-30 seconds per image for each filter. Data are collected at the characteristic auroral emission frequencies of 471, 486, 558 and 630 nm. The Meridian Scanning Photometers also operate at four different wavelengths, with two possible scan rates of either 180 elevations, twice per minute, or 17 elevations, once per minute. The overall set of optical data, combined with riometer observations from the same site, enables the mesoscale structure and the characteristic energy of the auroral particle precipitation to be mapped with good time resolution. The combination of the optical and riometer data with the overlapping data from the SuperDARN coherent radars and the CANOPUS magnetometer array also provides a very powerful tool to explore magnetospheric dynamics. See further notes about data combination in Section 6.

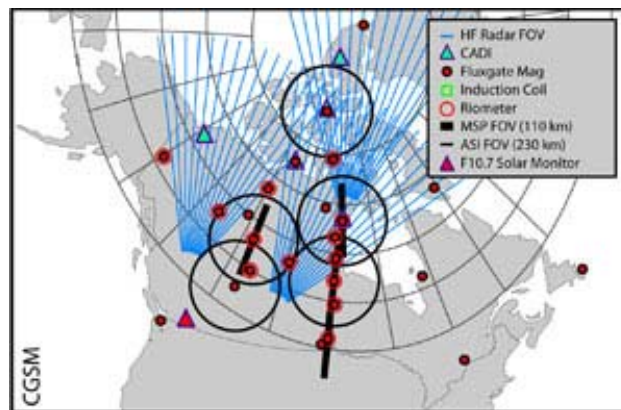
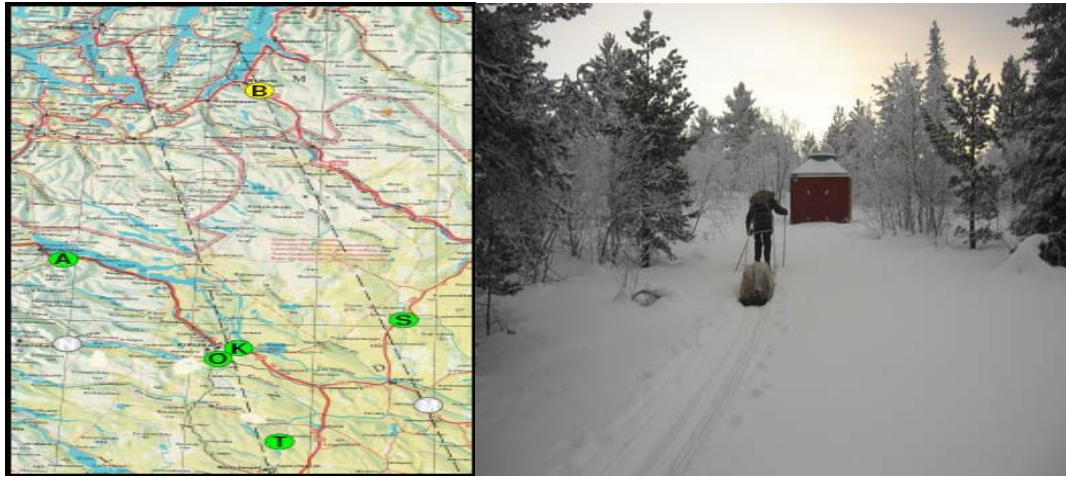


Figure 22: Location of the Canadian ground-based instrument network

The ALIS network of unmanned instruments in northern Scandinavia, which is no longer fully operational, utilised five fixed stations and one mobile instrument platform, separated by baselines of around 50 km. Each station contained a monochrome CCD imager, with a filter wheel containing up to six filters. All of the imager functions and pointing directions were under full remote control.



*Figures 23 and 24: Locations of the ALIS imagers, and one of the imaging stations.*

The use of co-located ASIs and MSPs seems to be a natural combination for a network of unmanned optical instruments. As well as aurora, these instruments are, in principle, capable of imaging airglow, but not of obtaining the neutral drift velocity in the same way as a Fabry-Perot Interferometer. FPIs are, however, completely capable of remote autonomous operation, and the NSF-funded Upper Atmosphere Facilities have operated FPIs for several years, in support of their incoherent scatter radars at Sondrestromfjord, Millstone Hill, Arecibo and Jicamarca. The combination of simultaneous neutral measurements of the temperature and dynamics of the neutral atmosphere is very powerful, making it a high priority to deploy such an instrument in association with the active EISCAT-3D site and preferably at all sites where there is not already coverage of the neutral atmosphere by an existing instrument. As mentioned in Section 3, the recent development of the Scanning Doppler Imager, essentially an FPI with all-sky imaging capabilities, suggests that SCANDI-type instruments might be a better choice than conventional FPIs for such an instrument network.

The number of passive optical instruments which might be deployed in association with the EISCAT-3D radars will be a function of the distances between site locations. Whereas simple instruments such as radiometers could be deployed at each EISCAT-3D site, many of the more advanced passive optical instruments have a relatively wide field-of-view, such that there would be no point in placing them too close together. Comparison with optical networks elsewhere in the world suggests that spacings for instruments such as ASIs and SCANDIs should be on the order of 1000km, meaning that such instruments could be deployed at the EISCAT-3D central site, and at the more distant of each pair of remote stations.

## 4.5 Passive Radio Instruments

This class of instrument includes GPS and beacon satellite receivers, ELF and VLF receivers, riometers and HF Doppler or passive radar systems. In most cases, the instruments are individually relatively cheap and the data requirements are not too stringent. Instruments such as GPS receivers are traditionally deployed in relatively dense grids (~100 km spacing) so that a receiver at each EISCAT-3D site can be regarded as a minimum, rather than a maximum requirement.

ELF and VLF receivers normally require radio-quiet sites, so that the naturally-occurring emissions from the ionosphere are not swamped by man-made signals. As such, these instruments are probably well-suited to being deployed at the EISCAT-3D remote sites, which are envisaged as unmanned remote locations, and not well suited to being operated at a busy central site. As noted in section 4.2, one option may be to keep one pair of remote sites as truly radio-quiet environments, in which case these sites would be well suited to the deployment of this kind of passive receiver.

The optimum spacing of riometers depends on the type of system selected. Single beam riometers could be closely spaced – however much better monitoring coverage could be obtained if the monitoring of cosmic noise absorption was carried out using imaging riometers, such as the existing IRIS system at Kilpisjarvi. In that case, a good solution might be to adopt the same deployment strategy as for the wide-field passive optical instruments, i.e. to deploy an imaging riometer close to the central site and a further imaging riometer system at each of the more distant remotes.

Passive radar systems, such as HF Doppler systems, could in principle be deployed at each EISCAT-3D site, and should certainly be strongly considered for sites where an active sounder (i.e. an ionosonde) is not being deployed. For sites where an ionosonde is deployed, some passive HF radar capabilities could in any case be retained by configuring the receiver so that it continues to scan between sounding transmissions.

## 4.6. Magnetometers

As noted in Section 3, magnetometers are perhaps the definitive network instrument, being normally distributed in geographic grids with baselines of order 100 km. Several magnetometers are already deployed for geophysical use in northern Scandinavia, as shown by the map in Figure 16, so that there is already good coverage of magnetic perturbations due to auroral processes in this region. Because the data rate from magnetometers is quite low in comparison to other instruments, however, we have assumed in this study that high-cadence magnetometers, suitable for pulsation studies, will be included at all of the EISCAT sites. In some cases, it might be more efficient for these to replace conventional search coil magnetometers already located near to the proposed sites.

## 4.7 Summary

Table 4.1 summarises the arguments outlined above, presenting in tabular form the possibilities for instrument deployment at the various categories of EISCAT-3D site. We divide the sites into three categories, namely “active” (the site hosting the

transmitter array”, “inner passive” (the closer pair of passive sites, assumed in this report to be radio quiet sites) and “outer passive” (the outer pair of passive EISCAT-3D sites, where active instruments of other kinds are allowed). The rows of the table show the different classes of instrument discussed above.

Instrument Type	Active Site	Inner Passive Site	Outer Passive Site
Coherent Scatter Radar	✗	✗	✓
MST/Meteor Radar	✓	✗	✓
Ionospheric Heater	✓	✗	✗
Advanced sounder	✓	✗	✗
Standard sounder	✗	✗	✓
HF Doppler	✓	✓	✓
LIDAR	✓	✗	✗
All-Sky Imager	✓	✓	✓
High-res auroral camera	✓	✗	✗
Spectrometer	✓	✗	✗
Airglow imager	✓	✓	✓
FPI	✓	✗	✓
Photometer/Radiometer	✓	✓	✓
GPS receiver	✓	✓	✓
Riometer	✓	✗	✓
VLF receiver	✗	✓	✗
Magnetometer	✓	✓	✓

Table 4.1: Possible supporting instrument complement for the EISCAT-3D sites

It is clear from this table that, if these recommendations were to be followed, the active site of EISCAT-3D would be extremely well-provided with supporting instrumentation, co-located to make combined observations with the radar. The inner passive sites would be much less comprehensively instrumented, with a relatively small number of passive instruments. In terms of their instrument complement, the outer pair of passive sites would be intermediate between the active site and the inner passive sites, with almost the same complement of passive instruments but also a number of active instruments, including coherent scatter and meteor/MST radars. It is not obvious that an MST/meteor scatter radar, or a coherent scatter radar, would be required at both of the outer remotes – but our working assumption is that one or other outer remote site should have at least one such radar.

## 5. Infrastructure and Data Rate Implications

In this section, we examine the implications of the instrument complements outlined in Table 4.1 for the infrastructure which is required at each site. As well as briefly considering the required physical infrastructure, we concentrate on the demands imposed by the volume of data from the supporting instruments and the implications which this has for networking and data storage. We then go on to consider the implications which these different data types will have for the operation and functionality of the central archive.

## 5.1 The Central Site

As outlined above, the EISCAT-3D central site is likely to be a very well-instrumented site, with a wide range of supporting facilities. We anticipate that there will be a co-located MST or meteor scatter radar for middle atmosphere studies, an ionospheric heater, and an advanced ionospheric sounder capable of providing MF radar and HF Doppler capabilities. In addition, there will be a wide range of optical facilities, including a sodium lidar, an all-sky imager (which should also have the capability for airglow imaging), an auroral spectrograph, a high-resolution auroral imager, an FPI or preferably a Scanning Doppler Imager, together with photometers or radiometers at a number of wavelengths. As well as the optical instrumentation, we envisage that there will be an imaging riometer, a dual-frequency GPS receiver and a high-specification magnetometer. This clearly requires an extensive site, although the EISCAT-3D array itself will be by far the largest user of space.

Because of the way that the central array of EISCAT-3D will be constructed, there should be ample opportunities to deploy other supporting instruments on the site. The largest part of the site will be given over to the central core of the active array, with elements possibly being arranged in a filled circle with radius of order 300m (see deliverable 4.2). However, the central site will also incorporate a number of small satellite arrays for EISCAT-3D interferometry (see the reports of Work Package 5), positioned around the central core, probably radiating outward in a spiral pattern. The total radius of the central site is likely to be upwards of 1km, but the outer portions of this will be only sparsely filled with outlier arrays, allowing plenty of space to deploy supporting equipment.

In order to obtain an initial estimate of the data rates and volumes associated with possible support instruments, we have reviewed the situation at a few key existing locations, including several of the existing ISRs which have support instruments clustered on their sites. In addition, a small number of installations have been purpose-built as STP observatory sites, though without incoherent scatter radars at the site. This enables us to get a good handle on the data flow and archiving demand, and outline the solutions which have been put into place to address this:

### 5.1.1 Other types of radar

Most of the coherent scatter radars currently operating in the world are built to a standard design. The SuperDARN radars typically consist of 16 horizontally polarised log periodic antennas, driven by a 600W transmitter, with a T/R switch which allows them to be used for both transmission and reception. A beam-forming network using fixed switched time delays allows the possibility to select any one of 16 beam directions. A further four, smaller, antennas are used to determine angle of arrival information. A standard seven-pulse transmission sequence is used to measure autocorrelation functions at a range resolution of 45 kilometres, and the phase information from an IQ detector is used to calculate the Doppler shift. The backscatter power and spectral width are taken directly from the autocorrelation function. This onboard data processing reduces an initially relatively large voltage-level data set to a very small set of summary parameters, which are the only results seen as scientifically worthy of preservation. The existing SuperDARN radars use dedicated phone lines to recover this prime parameter data from the various radar sites, meaning that the

bandwidth demand is only a few tens of GB per month, all of which should then be permanently archived .

The main data products from each SuperDARN radar comprise the so-called RTI (range-time-intensity) plots showing backscatter power and spectral width as a function of range and time, which can be inverted using a propagation model to show the geographic location from which such backscatter originates. Although there is no direct analogue to these quantities in terms of plasma parameters, it has been shown, for example, that the latitudinal boundary between narrow and wide spectral widths in HF coherent scatter data is a powerful indicator of the location of the Open-Closed Field Line Boundary.

As well as the data from each individual SuperDARN radar, some of the most powerful SuperDARN products are the so-called "SuperDARN mapped potential" plots (e.g. <http://superdarn.jhuapl.edu/rt/map/index.html>) where the line-of-sight velocity data from each radar are merged into an overall map of the high-latitude plasma convection, via the inclusion of a convection model driven by the solar wind parameters. Although the relative importances of the model and the measured data vary according to the amount of data available, the SuperDARN convection plots have become the standard tool in monitoring the convection of the high-latitude ionosphere.

The standard data products from MST radars are similar to those from coherent scatter radars - namely backscatter cross-section, spectral width, Doppler shift (with multiple estimates being combined into velocity vectors), and an estimate of aspect sensitivity derived using data from the sequential series of pointing directions. From these, one can obtain continuous profiles of the lower atmosphere wind, including the vertical components which reflect the dynamics of planetary waves and tides, and also map the location and structure in altitude of boundaries such as the tropopause and of meteorological phenomena such as weather fronts.

A state-of-the-art MST radar, such as that operated by the UK's Natural Environment Research Council at Capel Dewi, near Aberystwyth in Wales, has an array size of 110 x 110m. Within this volume is located a square array of 20 x 20 yagi antennas, at a spacing of around 5m. The peak transmitted power is around 160 kW at a maximum duty cycle of around 5%.

MST radars typically have four or five levels of data processing. In the UK MST radar described above, the lowest level data are the beam-formed "raw IQ" data, whose total volume is around 8 TB per month. This level of data is never recorded, however, but is coherently integrated in hardware to produce the second level "coherent IQ data", whose volume is about 16 GB per month. Even these data are normally only recorded by special arrangement. The first permanently recorded data are the spectral data consisting of 128 point spectra in each of around 150 range gates, with a typical time resolution of 20 seconds. It is considered essential to store the data at this level, but the volume is only around 8 GB per month.

The data required by most users are either the radial data, composed of key parameters derived from the spectral data, or the Cartesian data, formed by averaging the radial data over an entire pointing cycle. The processing to achieve each level

involves a factor 10 reduction in data volume at each stage, so that the radial data volume is about 500 MB per month and the Cartesian data volume is about 50 MB per month. The Capel Dewi MST radar uses a standard broadband line for all of its data products. Even if we were to store the coherently integrated I&Q data from an MST radar on the EISCAT-3D site, which the MST community does not normally consider necessary, the data volumes for transport and storage would be tiny fractions of those required for EISCAT-3D.

### 5.1.2 Ionospheric sounders

The data bandwidth required for handling ionosonde data depends primarily on the frequency at which successive soundings are obtained. Titheridge (1993) considered the data rate for a basic type of digital ionosonde (the KEL IPS-71) which simply records profiles of critical frequency as a function of height. He found that a single typical digital ionogram, obtained at 576 frequencies from 1 to 22.6 MHz and with 1.5km height resolution, occupied about 37 kB of storage. Even this was capable of being further compacted to between 5 and 9 kB per ionogram using standard run-length encoding. Since such ionograms are taken at typical resolutions of order five minutes, the bandwidth requirements of this kind of data are clearly trivial. The total annual data volume for one years worth of 5 minute ionograms from such a system was estimated to be no greater than 250 MB.

For more advanced ionospheric sounders, however, the data rate can be very much larger. When a system such as the EISCAT Dynasonde is operated in IDI (Imaging Doppler Interferometry) mode, an individual sounding can be as large as 1 MB, and such soundings can run at frequencies up to one sounding per minute (though one IDI mode sounding every ten minutes is more typical). At the highest rate, the total data produced by an advanced sounder would be of order 0.5 TB per year, still more than an order of magnitude less than the autocorrelated data volume from EISCAT-3D, but still a significant fraction of the total set of archived radar data.

HF Doppler systems usually exploit the reception of one or two fixed transmitter frequencies, using a relatively small spectral window for the receiver, centred on the nominal transmitted frequencies. A simple dual-frequency Doppler system reported by Chernogor et al (2002) used 10 Hz sampling on each channel, and computed Doppler spectra from each set of 512 samples, i.e. one Doppler spectrum per channel. Based on 8-bit sampling, this would give a data size of around 3 GB per day. However if there is not really any need to store the full data from each 0.1s spectrum, and the final data could probably be decimated by at least an order of magnitude. One way of achieving this would be to allow the information to be first written into the ring buffer where it could be temporarily stored during post-processing, with only the decimated output being written to the central archive.

Passive radars, if the kind described by Lind et al (1999) are receive-only systems, and typically require power supplies comparable to that of a standard desktop computer. Although they can operate on relatively small signal bandwidths, passive radars are most effective when large received signal bandwidths can be transported for subsequent correlation and signal processing. One passive radar experiment reported by Lind et al (1999) produced 3.6 GB of data in a six-hour period, equivalent to around 5 TB per year. Such data rates would make a significant impact on the data

rate at an EISCAT-3D site, and might be comparable to the data rate for autocorrelated data at the central site. It is unlikely, however, that a passive radar system could be operated at such a high data rate, since processing these six-hours of data in Lind's experiment with a modern quad-core computer required around one day of processing time. For these kinds of passive radars to be generally used, a better solution to the real-time data processing problem needs to be devised.

### 5.1.3 Active Optical Instruments

Lidars are powerful instruments for lower and middle atmosphere studies, but unfortunately their operation can generate very large initial data volumes. The LASE atmospheric lidar system developed by NASA incorporates 12 GB of associated storage, and a lidar study of lower atmospheric winds conducted in Oklahoma City by Calhoun et al (2006) generated over 100 GB of data during a 30-day campaign. The ATLID atmospheric lidar instrument currently proposed for the EARTH CARE satellite mission is proposed to produce a data volume of 12 GB per day, accounting for more than two-thirds of the spacecraft's data budget. However, these large file sizes can be reduced to quite small data sets of prime parameters. For example, a study done by the European Data Grid project time estimated the size of a month's worth of ground-based ozone lidar data needed for the validation of complementary space-based measurements at 2.5 MB.

From a data-taking point-of-view, lidars share many similarities with incoherent scatter radars. This is not surprising, because the techniques involved are very similar. Hence it ought to be possible to handle these data in a very similar way.

In Deliverable 8.3 from this work package, we have proposed a data-handling solution in which every EISCAT-3D site will be equipped with a ring buffer of several tens of Terrabytes capacity, sufficient to accommodate a few day's worth of sample level ISR data. These data would be held long enough for initial re-processing and would allow interesting periods of data to be held for longer periods to be re-processed in a number of different ways. The same philosophy could easily be applied to lidar data which, like ISR data, can be reduced from sample streams into smaller, higher-level data products. The size of lidar data indicated above means that the sample-level data would only consume a small fraction of the ring buffer, even if data from multiple different lidars were added simultaneously, and sufficient data processing would be available to comfortably re-process these data into higher-level products for transfer to the permanent archive before the use of buffer space became a problem.

### 5.1.4 Passive optical instruments

All-Sky Imagers are also capable of generating relatively large data volumes, because each image can be individually large, and images can be recorded at cadences of a few frames per second. For the storage capacities being discussed here, however, it is perfectly possible for auroral images to be stored in a small fraction of the disk space available at each site. For generalised auroral monitoring, Toyamatsu et al (2008) demonstrated the remote operation of an all-sky auroral camera whose images, obtained at 20s resolution could be stored in jpeg format, and amounted to a volume of around 80 GB per year (based on continuous autonomous operation, including during daytime). Although these were not really science-quality images, it was shown

that diffuse and pulsating aurora, as well as auroral arcs could be distinguished in the images which were obtained.

Science-class All-Sky Imagers typically record several frames per minute. For example, two All-Sky Imagers are deployed at the Gillam Auroral Station in Canada, one of which records two images per minute for an overall data rate of 11.1 kb/s, the other recording twelve images per minute for an overall data rate of 300 kb/s, which would be equivalent to around 25 GB/day (e.g. Trondsen, 2002).

At the highest data rates, auroral cameras move into territory where they can be considered as auroral video cameras, rather than true auroral imagers. The auroral TV camera at Sodankyla takes 25 frames per second, each frame consisting of 512 x 512 16-bit pixels,. The Swedish/UK ASK instrument on currently deployed in association with the ESR on Svalbard can record four frames of multi-wavelength data per second, creating 1.5 MB of data per second, and equivalent to 22 GB per hour. An auroral TV camera described by Trondsen et al (2002) taking 30 image frames per second creates 70 Mb/s of data, equivalent to 1.5 TB of data during a two-week campaign.

Of course, not all observations are of interest. The auroral season, even in northern Scandinavia is really limited from late September to early March, with the length of each night's observations being limited by solar zenith angle, moonlight and cloud cover. Even under clear conditions there is often little interest in keeping the highest time-resolution data unless active aurora are in the image field. In principle, therefore, auroral imagers are capable of producing data volumes anywhere between a few tens of GB to a few hundreds of GB per day, as we move from science-class auroral imagers up to highly capable TV-type systems.

For data storage, the same arguments apply as were described above in the case of lidar systems. Any auroral data could exploit the short-term buffering capability available at each EISCAT-3D site, allowing enough pre-processing to determine whether the observations were useful for further study. At remote sites, such buffering could be used to reduce the data rate sufficiently to either allow all-sky imager data from interesting intervals to be transferred along with the radar data, or to be subsequently transferred to local storage media such as large disks, which could be changed over during infrequent visits to an otherwise unmanned site.

If it is required to operate auroral TV systems or multi-wavelength imagers such as ASK in association with EISCAT-3D, in anything other than a campaign mode, the implied data rates would make it necessary for this to be located at an active site, which in any case, would be the most suitable location for such a highly capable instrument. In the case of continuous operations of such optical systems, one might expect that the integrated amount of such optical data will approach the integrated amount of auto-correlated data from the EISCAT-3D radar. No re-design of the basic data system structure is implied by this, but the presence of such optical systems on the site will be a powerful driver for the required volume of the available storage.

For spectrometers, airglow imagers and Fabry-Perot Imagers, integration times on the order of tens of seconds are typically necessary, reducing the data rate so that it becomes comparable with that of a normal auroral imager. Although these data are

not inconsiderable in size, they can be handled by being temporarily accommodated in the local ring buffer, at least until some consideration can be given as to whether further processing is needed. Cloud-affected images can be discarded, and even for good images, the image data does not necessarily have to be stored, since there is the capacity to reduce the data to a still smaller size, e.g. by only storing the properties of the spectral lines or the characteristics of the neutral velocity field (i.e. a representative number of vectors).

Because photometers measure integrated count rates, rather than multi-pixel images, their data are much smaller in size than those of all-sky cameras or FPIs. A typical atmospheric photometer system, such as those at Poker Flat or Fort Yukon, integrates for around one second on any given frequency, and cycles between four frequencies over a period of around eight seconds, including filter movements. Based on this type of cycle, the expected daily data size would be of order 10 MB per instrument. In the overall context of EISCAT-3D, this would be a very manageable data volume, so that it is entirely feasible to deploy multiple photometers for comprehensive wavelength coverage at all sites of the EISCAT-3D system.

#### 5.1.5 Passive radio instruments

Dual-frequency and other GPS receivers record their data in so-called RINEX files (Receiver Independent Network EXchange files). These are basically ASCII files, containing time, phase and pseudorange. The files can be compressed to a size of less than 1 MB per site per day, making them even smaller than the radiometer or photometer files discussed above. As before, the data rate produced by these instruments is not significant compared to the overall incoherent scatter data rate, and the daily RINEX data files can easily be moved around the EISCAT-3D network using the planned internet connections.

As described in section 4.5, the most capable riometers are the multi-beam imaging instruments, which are becoming widespread for the measurement of the geographic distribution of Cosmic Noise Absorption. Typically, imaging riometers are of one standard type (known as IRIS riometers) which provide cosmic noise levels on each of 49 beams, with each beam being sampled once per second, and the data written out to a binary format data file. The resulting daily data file is around 7 MB in size, making it one of the smaller data sets likely to be collected in association with EISCAT-3D.

Because of the large area covered by multi-beam riometers, it is unlikely that such an instrument would be required at each EISCAT-3D site. The most comprehensive coverage would be obtained by using an imaging riometer at the central site and at each of the further remotes, but even this may be unnecessary. Possibly one imaging riometer covering the whole area of the EISCAT-3D array and supplemented by single-beam riometers (with a 49 times lower data rate) at the remaining sites would be an entirely acceptable solution. In any case, the data rate implications of operating riometers in conjunction with EISCAT-3D do not appear to be severe.

Although these are relatively simple receiver systems, the data rate from VLF and ELF receivers can be quite large, depending on the bandwidth of the received signal and the frequency with which data are saved. One of the most up-to-date VLF/ELF

receiver systems is the AWESOME receiver, produced by Stanford University (see [http://solar-center.stanford.edu/SID/AWESOME/docs/AWESOME\\_preparations.pdf](http://solar-center.stanford.edu/SID/AWESOME/docs/AWESOME_preparations.pdf)). In this system, the data rate can be up to 1.5 GB per hour, if the full broadband data are accumulated continuously. However, the system is normally only operated in this mode during special campaigns. In normal synoptic observations, broadband data are recorded for only one minute out of every 15, with the remaining 14 minutes being used to record narrow-band data, where the amplitude and phase of a single frequency corresponding to a VLF transmitter is monitored. This effectively reduces the data rate by around an order of magnitude, producing a data volume of order 5 GB per day. This is still an appreciable size, significantly greater than GPS receivers or riometers, but significantly less than the really large data sources such as auroral TV systems or lidars. Particularly in the broadband data, there is likely to be a possibility for appreciable data compression, meaning that data could be added temporarily to the cyclic buffer to allow suitable compression algorithms to be applied, before being written to a final form which would allow the data to be transported off-site into the central store.

#### 5.1.6 Magnetometers

The Canadian CARISMA magnetometer array samples at a basic time resolution of 8 Hz, which is initially stored locally on a data logger. Because of the remote locations of several of these magnetometers, a direct data uplink to communications satellites is used to disseminate their data via a satellite internet link. In the case of EISCAT-3D an 8 Hz sampling increment represents a trivial amount of bandwidth in relation to the total volume coming from the radar remote sites. Assuming this sampling rate applied to three independent directions with 16-bit sampling gives a data size of around 30 MB per day, which is trivial compared to many of the instruments mentioned above.

### 5.2 **Supporting instruments at the remote sites**

As set out in section 4.7 and summarised in Table 4.1, the complement of supporting instruments envisaged for the EISCAT-3D remote sites is largely a subset of the supporting instruments at the central site. The scenario we have examined here is that the EISCAT-3D system will have four remote sites, of which the two inner ones will be kept “radio quiet” (i.e. no active radar instruments) in order to allow the deployment of sensitive instruments like ELF and VLF receivers. At these inner sites, there will be comparatively few supporting instruments, and all of them will be essentially passive systems. The envisaged complement for each of the inner remote sites comprises an HF Doppler receiver, an all-sky imager, an airglow imager, a (multi-frequency) photometer or radiometer, GPS and beacon satellite receivers, ELF and VLF receivers and a high-specification magnetometer.

All of the above instruments, except for the ELF and VLF receivers, are then duplicated at the outer pair of remote sites. Because there is no requirement for these to be “quiet” sites, it is suggested to operate an ionospheric sounder, an MST or meteor scatter radar, and possibly a coherent scatter radar at each of the outer remotes. It is also envisaged to operate a Fabry-Perot interferometer at each of the outer remote sites, the assumption being that these instruments would have a sufficiently large field-of-view that, together with the FPI at the central site the three instruments would

make observations of the neutral dynamics over the whole EISCAT-3D network, including tristatic observations of the neutral wind (a capability which has been unique to EISCAT until recently, because of the FPIs already deployed at Tromso, Sodankyla and ESRANGE).

Some of the most complex instruments with the largest data rates, such as advanced ionospheric sounders, high-resolution auroral imagers, spectrometers and lidars would be reserved for the central site. This stands to reason because these instruments require frequency manual intervention and continuous high data rate connections to the central archive. These things cannot be provided (or at least cannot be guaranteed) at the remote sites, which are designed for long-period unattended operation and for which there is a fairly high possibility that breaks in communication with the central archive will result in data having to be stored on site for extended periods.

### **5.3 Summary of data rates and infrastructure requirements**

In Tables 5.1 and 5.2, we have tried to capture all of the data storage implications from the supporting instruments envisaged for EISCAT-3D, on the basis of the survey of data rates from existing instruments reported in Section 5.1. These tables refer to the central site and to the remote sites, though in Table 5.2 we also distinguish between the inner and outer remote sites.

The second column of each table demotes the data rate produced by the instrument, ahead of any pre-processing that we might wish to do before ingesting the data into the permanent central archive. In these tables, we have expressed all data volumes in units of GB per day, which seems the most appropriate unit especially for the more data-intensive instruments. Some of the instrument data rates are trivially small on this scale, often because they consist of no more than digitised streams of measurements of single (or a few) variables. In some cases, e.g. for coherent scatter and meteor radars, the input data rates may seem surprisingly small, but this is because these instruments come with their own purpose-built computer systems which carry out functions such as data decimation, integration and signal processing before the data are output to any other system. In such cases, we assume that no further post-processing will be done, and that the data can simply be output to the central archive.

The third column of the tables indicates what type of access is required in order to connect the supporting instrument to the EISCAT-3D data system. The use of “CA” means that the instrument has a direct network connection to the central archive, which is the case for all instruments which carry out their own pre-processing, or for those in which the data rate is too small for post-processing to be needed. The use of “RB” means that the instrument is connected to the ring buffer in the first instance, usually because the initial data set is large and can be reduced in volume by post-processing which is not handled by the instrument itself. The most obvious example is in the case of the various types of imager, where data sizes can be reduced dramatically by eliminating any images obtained during cloudy periods or (in the case of auroral imagers) during periods of no aurora.

Instrument Type	Data rate per day (GB)	Access Required	Archive data rate per day (GB)	Comments
Coherent scatter radar	-	-	-	-
MST/Meteor scatter radar	0.5	CA	0.5	Record coherent IQ
Ionospheric heater	-	-	-	-
Advanced sounder	1.5	CA	1.5	Based on Tromso Dynasonde
Standard sounder	-	-	-	-
HF Doppler	3	RB	0.3	Decimation in ring buffer
Lidar	4	RB	<<1	Post-processed in ring buffer
All-sky imager	25	RB	~10	Only save clear and auroral periods
High-res auroral camera	250	RB	~100	As above
Spectrometer	25	RB	~10	Comparable to auroral imager
Airglow imager	25	RB	~10	Could be same instrument as auroral imager
FPI	25	RB	~10	Comparable to auroral imager
Photometer/radiometer	<<1	CA	<<1	
GPS receiver	<<1	CA	<<1	
Riometer	<<1	CA	<<1	
VLF receiver	-	-	-	-
Magnetometer	<<1	CA	<<1	
GRAND TOTAL	~350		~150	

*Table 5.1: Data volume implications of instruments at the central site*

Instrument Type	Data rate per day (GB)	Access Required	Archive data rate per day (GB)	Comments
Coherent scatter radar	2	RB, CA	2	Outer sites only
MST/Meteor scatter radar	0.5	RB, CA	0.5	Outer sites only. Record coherent IQ
Ionospheric heater	-	-	-	-
Advanced sounder	-	-	-	-
Standard sounder	<<1	RB, CA	<<1	Outer sites only.
HF Doppler	3	RB	0.3	Decimation in ring buffer
Lidar	-	-	-	-
All-sky imager	25	RB	~10	Only save clear and auroral periods
High-res auroral camera	-	-	-	-
Spectrometer	-	-	-	-
Airglow imager	25	RB	~10	Could be same instrument as auroral imager
FPI	25	RB	~10	Comparable to auroral imager
Photometer/radiometer	<<1	RB, CA	<<1	
GPS receiver	<<1	RB, CA	<<1	
Riometer	<<1	RB, CA	<<1	
VLF receiver	5	RB	1	Decimation in ring buffer
Magnetometer	<<1	RB, CA	<<1	
GRAND TOTAL	~100		~30	

*Table 5.2: Data volume implications of instruments at each remote site*

At the remote sites every instrument, regardless of its data volume, is assumed to have a connection to the local ring buffer, even if it also has a direct connection to the central archive. This is done in order to allow for periods of network outage, during which data from supporting instruments can be accumulated for some period of time in the ring buffer, even if no pre-processing is needed, until network connectivity is restored. At that time all of the data temporarily held in the ring buffer are copied to the central archive. Of course, any data from supporting instruments would only be stored for an extended period in the ring buffer as long as such storage was consistent with the prioritisation scheme under which the use of the ring buffer is allocated. This issue has been extensively discussed in Deliverable 8.3.

The fourth column of the tables reflects the data rates for the relevant instruments which will flow out of the ring buffer and into the central archive, this is equivalent to the amount of data for each instrument which will be permanently stored. Where this figure is not the same as the figure in the second column, it reflects our estimate of the amount of data reduction which can be achieved by pre-processing the data in the ring buffer. The totals shown in the bottom row of each table reflect the fact that we can conservatively expect to achieve a factor 2 in data reduction by implementing such pre-processing strategies. The fifth column contains comments specifying which strategies might be most appropriate.

#### **5.4 Discussion**

From the figures shown in Tables 5.1 and 5.2 we can deduce that, if we deployed the entire complement of supporting facilities suggested in this report, the effect would be an input to the central site ring buffer of about 350 GB per day, an input to the remote site ring buffers of about 100 GB per day, and an input to the central archive of order 300 GB per day, due to data from the supporting instruments alone. The figure for the data input to the central archive assumes that supporting instruments at the central site contribute 150 GB per day, with of order 30 GB per day coming from each of four remote sites.

In terms of current STP facilities and their associated archives, the idea of producing more than 1 TB per week of data from supporting instruments alone seems rather alarming. (For comparison the current EISCAT raw data archive at RAL is less than 20 TB, acquired over a period of more than 20 years). However, if we compare with the figures given in Deliverable 8.3, relating to the storage of data from EISCAT-3D itself, we find that the projected rate of growth for the permanent central archive is 200 TB per year (or around 4 TB per week). Hence the data from the entire complement of supporting instruments suggested here would only be of order 25% of the size of the data archive from the EISCAT-3D radars themselves, which seems to be a perfectly acceptable overhead for the potential increase in scientific return.

In terms of the ring buffers it can be assumed that, excluding network outages, there will be no long-term accumulation of supporting instrument data in the buffers – i.e. the input data are deleted after pre-processing, and the pre-processed data are shipped out directly to the central archive. In any case, the size of ring buffer required to store 24 hours of EISCAT-3D raw data is of order 70 TB (see deliverable 8.3, p84) meaning that the temporary storage and input data rate demands on the ring buffer for the supporting instruments are miniscule compared to the data traffic through the ring buffer generated by EISCAT-3D. In principle, this could allow data from the supporting instruments to be accumulated in the ring buffer for quite long periods (weeks) if the need arose. This situation arises because the supporting instrument data are fundamentally different from the EISCAT-3D raw data, in that in EISCAT-3D the sizes of raw to pre-processed data are in the ratio of around 100:1, whereas for the supporting instruments this figure is more like 3:1.

#### **6. Data combination and Value-Added Products**

Most of modern space science is inherently based on multi-diagnostic observations. This means that single-instrument data sets are rarely used in isolation, and much of

the newest and most interesting science comes from the use of multiple data from different instruments. Frequently, this involves only the comparison of data from different techniques, to answer questions such as:

- What are the characteristics of the ionosphere within and adjacent to an optical aurora?
- What are the comparative parameters (density, temperature and velocity) of the ionised and neutral atmosphere within a given volume ?
- How do the features seen by different types of radars relate to each other (e.g. what is the significance of spectral width boundaries seen in coherent scatter data, in terms of the plasma parameters measured by incoherent scatter data ?)
- What effect does high-energy particle precipitation (as measured by incoherent scatter) have on the middle atmosphere column densities of nitrous oxide and ozone (as measured by photometry) ?

In the above cases, a simple comparison of data products from different instruments is all that is required to advance scientific understanding. The data products produced by the various different instrument types have already been reviewed as part of Section 3. In some particular cases, however, it is possible to combine data from different instruments to produce new “value-added” parameters which can be added to the archive in their own right. In this section, we briefly review such possibilities, looking at the parameters which could be generated by combining data from the different instruments within the EISCAT-3D “observatory” and those which could be obtained by combining with data taken over a wider geographical area.

Before discussing these value-added data products further, it should be mentioned that these are among the highest-level data products which will be produced by EISCAT-3D, and consequently most of these data sets will be very small. In terms of their impact on the size and throughput of the archive, these data are not significant. However they are important in terms of the scientific value which they will add to EISCAT-3D as a facility.

## **6.1 Vector velocity combinations**

Perhaps the most obvious example of data combination is the combination of multiple radar measurements of line-of-sight velocity into full three-dimensional vector velocity estimates. In the non-collisional ionosphere (e.g. above 150 km) the electrons and ions move with a single plasma velocity, so that observations of three components of this velocity along different lines of sight can be combined into a single vector. This procedure is already routinely carried out for common volume measurements from the three sites of the EISCAT UHF system, but common volume measurements are not strictly necessary. As long as the velocity field above a given radar site is spatially homogeneous over a reasonable area, and constant over a reasonable length of time, a vector determination can be made by combining simultaneous (or closely sequential) velocity measurements in different directions from the same site. A multi-beam system such as EISCAT-3D would obviously be well-suited to this kind of determination, and indeed the possibility would exist to carry out different kinds of “beam-swinging” velocity determinations to those which are currently possible, e.g. by using multiple redundant sets of beam directions in different parts of the observing volume, to produce maps of the velocity field around

the location of the radar site. With some assumptions about the vertical velocity, and the use of continuous range-gated velocity measurements from multiple low-elevation beams, the velocity can be mapped over a wider area.

The ability to measure multiple simultaneous beams would not only allow multiple over-determined estimates of the F-region plasma velocity, but by using multiple beams from the remote sites, projected into the transmitter beam at different heights, it would make it possible to measure complete altitude profiles of vector velocity, to investigate the transition between F-region conditions, dominated by the electric field, and collisional E-region conditions, where the velocity is dominated by the neutral wind.

The technique of velocity combination is not limited to data obtained by an incoherent scatter radar. In principle, a number of the instruments associated with the “EISCAT-3D observatory” could contribute velocity data which could be combined vectorially. A similar technique is already used in the case of Dynasonde data, where Doppler shifts associated with individual echo regions are combined to produce drift velocity vectors. Velocities are also measured by coherent scatter radars, where multiple beams are used and the data inverted to produce a velocity field. In the lower ionosphere, MST and meteor radars are routinely used to measure velocities, especially extended measurements of vertical velocity for the study of phenomena such as planetary waves and tides.

Given the number of different observing techniques described above, one could anticipate a very rich velocity data set, mapping the plasma velocity field at a wide range of altitudes from the F-region down into the E-region.

## **6.2 The Ion-Neutral Difference Velocity**

The difference velocity between the ionised and neutral atmosphere is a key parameter for calculating the electrodynamics of the high-latitude upper atmosphere (see below). Given the ability of EISCAT-3D to image the entire plasma velocity field above the radar, a similar capability to measure the entire neutral velocity field at a range of altitudes would be a very major benefit. This kind of spatial information is not really available from the present generation of IS radars, due either to their inability to map the velocity field, or because the required supporting instruments are not available.

For the mapping of the neutral velocity field, an instrument such as a Scanning Doppler Imager is required (see Section ??), but this would need multiple filters in order to image both E and F region emissions, which would enable the altitude variation of the neutral velocity to be predicted.

## **6.3 Electrodynamic parameters**

Incoherent scatter radars have, in principle, a unique capability to measure E-region parameters such as the ion-neutral collision frequency, although this calculation frequently requires the combined use of data and models (see below). The ion-neutral collision frequency is a very important measurement, because its magnitude determines the extent of the coupling between ionised and neutral components of

the upper atmosphere, and its measurement (along with the measurement of the plasma density profile and modelling of the electron-neutral collision frequency) allows the determination of electrodynamic parameters such as the Pedersen ( $\sigma_p$ ) and Hall ( $\sigma_H$ ) conductivities and currents, the Poynting Flux  $\mathbf{J} \cdot \mathbf{E}$ , the Joule heating rate  $\mathbf{J} \cdot (\mathbf{E} + \mathbf{U} \wedge \mathbf{B})$  and the Lorentz forcing of the ionosphere on the neutral atmosphere  $\mathbf{U} \cdot (\mathbf{J} \wedge \mathbf{B})$ .

In conventional incoherent scatter radars, these parameters are produced by combining direct measurements with simply derived parameters such as vector velocities. Strictly speaking, these parameters can only be measured at a limited set of locations determined by the beam pointing directions. However, distributions of these parameters can be calculated if enough spatially-separated observations can be obtained to allow the distributions of density, collision frequency and velocity to be calculated. A phased array multi-beam radar would lend itself well to this kind of study. In addition, Kosch et al (1998) have shown how Pedersen conductances (i.e. height-integrated Pedersen conductivities) can be estimated using all-sky imager data at 557.7 nm. They also show that the technique can be extended to measure Hall conductances, but in this case dual-wavelength imager measurements are required, due to the greater dependence of the Hall conductivity on particle energy. Although their method only allows the measurement of height-integrated conductivity, its power is that it uses image data to measure the conductance distribution simultaneously over a two-dimensional field.

#### **6.4 Neutral Temperatures**

If the ion temperature, the ion-neutral difference velocity and the ion-neutral collision frequency are known, or can be well modelled, the neutral temperature can also be calculated from simple energy balance arguments. However, the neutral temperature can be estimated by some other instruments in the “EISCAT-3D observatory”, including Fabry-Perot Interferometers, where information on the neutral temperature can be gained by measuring the line width of the various emission lines. As in the cases above, the power of combining EISCAT-3D data with data from the various auxiliary instruments would permit not only multiple estimates of the same parameters, but also offer a method of generalising a few validated single point measurements to a field corresponding, for instance, to an imager field-of-view.

#### **6.5 Ion and neutral composition**

In principle, the ion composition can be recovered from well-determined incoherent scatter spectra. In practice, however, it is very difficult to distinguish changes in ion composition from those in ion temperature, and since the latter parameter varies more dynamically, it is conventional to fit for ion temperature, while modelling ion composition. In EISCAT-3D, we expect to be able to determine the ion line spectrum very accurately, thanks to the radar's high figure of merit. However EISCAT-3D will also provide detailed observations of plasma line, giving an independent measurement of electron density, which can be fed in as a priori information to reduce the uncertainties in the ion line fitting, and giving more accurate fitting of the ion composition. This method has already been used at Arecibo, by Aponte et al (2007), and builds upon a method originally developed by Waldteufel (1971).

## **6.6 Heat flux, suprathermal electrons and plasma lines**

It is long been realised that the size and anisotropy of the suprathermal electron flux can be determined from the strength of the plasma lines measured by incoherent scatter radar. The effect arises because a change in the electron energy spectrum can affect the growth or damping of the Langmuir waves which give rise to the plasma lines, either weakening the plasma lines, or enhancing them above the thermal level. The relationship was calculated in detail by Bjorna and Hansen (1986) and although difficult to measure, the effect can be important because of its potential ambiguity with the effect of an ionospheric current, which can also cause an additional Doppler shift in the plasma lines. The position of the plasma line is also sensitive to the altitude gradient of electron temperature, which affects the dispersion relation of the Langmuir waves and in principle this enables the plasma lines to be used to measure electron temperature and heat flux in the electron population.

While the plasma lines can yield some important information, the routine retrieval of these parameters is almost never done, partly because the quality of plasma line measurements often does not permit it, but also because of the amount of assumptions and supporting modelling which are required. In principle, EISCAT-3D could allow very detailed and accurate plasma line measurements, removing the first problem, while the second problem could be improved by routine access to a powerful computer system deployed in association with the data archive.

## **6.7 Potential patterns from radars and magnetometers**

The specification of the high-latitude potential pattern is a key parameter in polar geophysics, since the determination of these patterns provides information on the convection pattern as well as the location and direction of current systems, including field-aligned currents. A number of methods already exist which merge multi-diagnostic information to produce convection patterns and potential maps, and the wide coverage available from EISCAT-3D will make it an important contributor to studies of this kind. The AMIE technique (Assimilative Mapping of Ionospheric Electrodynamics) uses a constrained least-squares fit to a range of observations from different instruments including magnetometers, satellites, coherent scatter radars and incoherent scatter radars. An underlying model due to Weimer (1996) is used, which is driven by upstream IMF and solar wind conditions. Ground-based measurements of magnetic disturbances are used to compute global-scale Hall and Pedersen conductance distributions and these, with other input information are used to adjust the background potential and conductivity patterns. The procedure of data assimilation and re-computation is repeated with a one minute time-step. AMIE has proven to be a very powerful technique for the interpretation of STP data, though it is constrained by the lack of data availability in some longitude sectors, and by the inherent limitations of the underlying model, which breaks down during very active periods.

In the SuperDARN map potential method (Ruohoniemi and Baker, 1998), equipotential contours are determined by fitting a series of spherical harmonic functions to the convection velocity components measured by the global network of SuperDARN radars. In regions where there is little or no data, the fits are constrained by statistical models based on upstream IMF conditions. In the ionosphere the

equipotential contours are also velocity streamlines, so that the global-scale voltage maps are equivalent to global-scale convection maps. Although the input data are dominated by measurements from coherent scatter radars, there is no reason why this should be the case, and the EISCAT radars have contributed velocity measurements to be used in this technique. Because of the capability of EISCAT-3D for rapid beam scanning, the velocity maps produced by the new radar will be more similar to those produced by coherent scatter radars, making them highly suitable as input to these potential mapping applications.

### **6.8 Energy Maps using radars, imagers and riometers**

The calculation of “energy maps” (geographical distributions) of the characteristic energy of precipitating particles) is of great importance for ionosphere-magnetosphere coupling studies, since the estimation of field-aligned currents requires good information about the distribution of ionospheric conductances and their spatial gradients. For this kind of application, riometer and auroral imager data, both of which have extensive geographical coverage, can be combined together to produce large-scale energy maps. Kosch et al (2001) have shown that the characteristic energy can be derived by dividing the scaled riometer absorption measurement by the square root of the intensity of the green line optical emission at 557.7 nm. However, the method still has to be independently calibrated using incoherent scatter radar, as the only instrument capable of measuring the full electron density profile.

The potential patterns and energy maps described in the two sections above are closely related, since the extent of ionosphere-magnetosphere coupling, which determines the convection pattern, is itself determined by the distribution of the conductivities (which represent another aspect of the coupling). More work needs to be done in computing and inter-comparing these types of product, in order to optimise the use of all the available multi-instrument data to produce the best estimation of the coupling between the ionosphere and magnetosphere. The EISCAT-3D data system can play an extremely valuable role here, not only by bringing together all the relevant data sets, but by providing the necessary computing power to combine these data in the required manner, and to evaluate the success of such combination techniques.

### **6.9 Tomographic images and their calibration**

Networks of GPS receivers, or other types of beacon satellite receivers, are able to make continuous measurements of received signal phase, whenever a suitable satellite is in view. The phase delay imposed by the ionosphere depends on the line integrated electron density between the satellite and the receiver and, since the satellites are continuously moving with respect to the receiver, the receiver networks continuously make measurements of the Total Electron Content on a succession of changing raypaths. These multiple estimates can be input into inversion algorithms to produce wide-area tomographic maps of the global distribution of electron density. The technique is limited in resolution by the spacing of the receiver network, becoming increasingly unreliable over the poles and oceans, where Kalman filtering is used to model the evolution of the plasma density between well-instrumented areas.

In the case of single frequency beacon satellites, only the relative phase difference can be measured as the satellite moves over the receiver network. The phase of the beacon signal has already undergone a large integer number of rotations during its passage through the ionosphere – however this number is unknown. Because of this, only relative density is recovered, and the map needs to be calibrated by an incoherent scatter radar, which can actually measure the TEC along the beam. In the case of GPS, two beacon frequencies are available, as well as encoded information about the transmission time, which make it possible to infer the total amount of Faraday rotation. However, GPS tomography is mainly based on the inversion of slant ray paths, and measurements of vertical TEC, such as those provided by a radar, are still of great importance for the validation of the final tomographic image.

As we have seen, therefore, the combination of EISCAT-3D's incoherent scatter data with complementary data from the other instruments of the EISCAT-3D observatory (and over a wider geographical area) can be used to provide a wealth of contextual information about the morphology of the high-latitude ionosphere and its connections to the magnetosphere. Bringing all of this information together, and making the various data products self-consistent will be a very interesting challenge in using the data from the new radar.

## **6.10 The importance of models**

Of course the over-riding purpose of EISCAT-3D is to advance our understanding of the physical processes which control the upper atmosphere and determine its coupling to the regions above and below, so that we can identify the most important processes and predict the future development of the coupled system. This is an ambitious goal, which cannot be addressed using data alone. In order to demonstrate our understanding, we must be able to use our data to build improved models of the magnetosphere-ionosphere-atmosphere system, and then show that those models can be successfully used to predict the future evolution of the system in a manner validated by subsequent observations.

Upper atmosphere modelling is already several decades old, and there are a number of physics-based models which predict the state and development of the upper atmosphere independently of any observations. As we have seen in the sections above, the potential exists to derive a large number of physical parameters from the observations made by incoherent scatter, but this often cannot be done unambiguously from the data alone. In many cases, additional parameters are taken from models in order to allow other parameters to be derived from the observations. An obvious example is the modelling of ion composition which is needed to recover the ion temperature from the F-region ion line spectrum, or the modelling of the ion-line collision frequency needed to recover the E-region plasma temperature. There are also more complex cases, such as the modelling of the electron-neutral and ion-neutral collision frequencies to provide conductivities and current densities, which lead into Joule heating and Lorentz forcing rates. Of course, the rationale for modelling the ionised and neutral upper atmosphere is not just to better interpret our observations, but also because such modelling helps us to understand the reasons for the variations which we observe, and predict how they will continue into the future.

Unfortunately, the current generation of physics-based models has only a very limited ability to make accurate predictions of the state of the high-latitude ionosphere. Even in situations where the measured state of the ionosphere is used as a starting point for the model, most models cannot predict the subsequent development of the ionospheric morphology on any period beyond a day or two, even if the appropriate solar and magnetospheric activity indices are used as input parameters. This lack of success of current physics-based models encourages the belief that some important processes are still not correctly handled. One of the likely areas of weakness in the present generation of models is their limited handling of non-linear processes, which allow initially small perturbations eventually to produce substantial effects.

In order to improve the reliability of our current models, and to better understand their present shortcomings, there has been considerable activity in developing a new generation of assimilative models, where the purely physics-based modelling is supplemented by a continuous confrontation with real, measured data. These allow the state of the model to be updated via some kind of “observation matrix”, which constrains the model towards the real, measured values using some kind of multi-variant minimisation technique.

The best known of these models is GAIM (the Global Assimilative Ionospheric Model) which has been developed since 1999 under a programme sponsored by the US Department of Defense. This is a 3-d, time dependent model, based on first-principles physics techniques, which solves numerically for the ion and electron density. The model also includes state-of-the-art optimisation techniques, including Kalman filtering and 4-dimensional variational approaches, to assimilate measurements such as line-of-sight TEC estimates and density profiles obtained from ionosondes and incoherent scatter radar. Two simpler assimilative models, developed in an attempt to improve the prediction of ionospheric profiles for the communications community are EDAM (the Electron Density Assimilative Model, developed by Qinetiq in the UK) and IonoNumerics, developed by Fusion Numerics Inc., under contract with the United States Air Force Research Lab. IonoNumerics is a physics-based model capable of assimilating slat TEC measurements from ground-based GPS receivers, while EDAM is a climatological model which uses TEC measurements to adjust empirical electron density distributions.

The reason for introducing assimilative modelling into the present discussion is to make the point that, as well as being a vital underpinning of EISCAT data interpretation - especially for inferring the indirectly derived parameters – there is another aspect of the relationship between data and models, which will become increasingly important. Solar-Terrestrial Physics has moved from being a primarily observational science to being a true synthesis science where both modelling and data play a strong role in advancing our understanding. This means that model and data sources are becoming increasingly tightly connected – with parameters from the model being carried over into the data analysis, while parameters from the EISCAT data set, and from the other observing instruments deployed in association with the radars, will be used to constrain the model. As predictive capabilities improve, the models will inevitably play a stronger role in providing alerts to change observing modes and schedule different kinds of operations. This has significant implications for the way that the computer system and the data archive will be configured at the central site, and these are explored in sections 8 and 9.

## **7. Data distribution techniques**

As noted in the previous deliverables of this work package, data distribution is a key issue for EISCAT-3D at a number of different levels. Data distribution within the array is the most critical in terms of time and speed, but this is dealt with by Work Package 12. In Work Package 8, one critical issue is that of the distribution of data *between* the different sites of EISCAT-3D, particularly between the central site and the remote arrays, but also the data flow at the central site, particularly the data traffic into and out of the co-located permanent archive. In Section 3.4.5 (pages 86-87) of Deliverable 8.3, we have reviewed the network bandwidths required to handle the flow of EISCAT-3D between sites, suggesting a requirement for 2.6 Gbits/s to connect the central and remote site ring buffers, with no allowance for protocol overhead. In subsequent discussions, we have specified a requirement for a 10 Gbit/s dark fibre network at each of the sites. Below, we show that this bandwidth should be comfortably enough to handle all of the archivable data from the EISCAT-3D remote arrays, together with the archivable data from the other supporting instruments deployed at each site, assuming that there is a capability for some of these to access the cyclic ring buffer for initial temporary storage of their rawest data, so that these could be post-processed into the higher-level data products which would then be transferred to the permanent archive.

When considering how EISCAT-3D data and the data from the supporting instruments should be stored, we have to take account of the subsequent requirements for accessing these data, since our aim is to provide the highest possible capability, in terms of easy, user-friendly data access to our scientific user community. In this respect, the requirements at the remote sites are very different from that at the EISCAT-3D central site, where the master archive will be located.

At the remote sites, we have assumed that there will not be a requirement for high-level data access direct to science users. The main requirement will be to ensure a safe, fast and effective transfer of data from the remote site to the central archive. In Deliverable 8.3, there is considerable discussion of how this will be achieved.

The ability of globally distributed users to have full, equal and open access to all of the data from the central archive will be crucial to the success of EISCAT-3D. There are a number of ways that this can be achieved, but the most future-proof method is likely to be via the use of grid or virtual observatory (VO) technology.

The aim of a virtual observatory is to provide seamless access to data irrespective of its location, the aim being for any scientific data set to be accessible to users of a virtual observatory in the same way that any web page is accessible to a user of the worldwide web. In the VO world, data sources are widely distributed, typically being held in well-found archives close to the point of production, where they can be curated by people who are specialised in their use and interpretation. The central archive of EISCAT-3D would be an example of one such archive, but a VO user would have similar access to any other archive, such as the archive holding data from another incoherent scatter radar, or another multi-diagnostic instrument cluster.

At each archive, the local staff maintain a DSA, a data set access program, which is effectively an up-to-date directory of all the data held in the archive, and how it is stored. Within the VO environment, it is possible to formulate a large number of queries and searches, depending on what the user wants to do with the data – options can range from simple data discovery to event searches to various types of data combination. All of these queries are based on generic VO protocols, but are format agnostic – i.e. they do not care in which format the underlying data are stored. The job of the DSA and associated applications such as PLASTIC (insert definition here) are to convert these generic calls into the specific syntaxes used in the database, so that they can be locally implemented.

This means that there is considerable freedom for the local archive to be structured in whatever way is most convenient – the actual format is invisible to the VO user, who only interacts with the archive via PLASTIC-type VO programs, mediated by the information contained in the DSA.

There is already considerable experience of making archive data from incoherent scatter radars and other types of STP diagnostic available within a VO environment. A copy of much of the analysed data from the current EISCAT central archive is routinely made available via Madrigal, a distributed archive system developed in the United States. Madrigal is an open-source product (see [www.openmadrigal.org](http://www.openmadrigal.org)) whose underlying software is available for public download, allowing any user to start his or her own madrigal site and to populate their own database implementation with data from their local instrument. Madrigal uses a version of the NCAR CEDAR data format, developed at the National Center for Atmospheric Research in Boulder, Colorado. The format provides for an arbitrary number of 1D and 2D data variables, each identified by an extensible central code list, as well as providing for centi-second time resolution and a range of quality parameters to show goodness of fit, residuals, standard errors etc.

Madrigal databases now exist at around a dozen sites worldwide, including EISCAT, and the whole ensemble of databases can be queried centrally, so that users searching for a particular data set do not need to know in which of the archives it is actually located. In this sense, Madrigal functions rather like a Virtual Observatory, although with less generic capability because functions such as data searching are restricted to other Madrigal archives.

In conjunction with the FP6 funded EURO-VO project, and with the participation of people involved in WP8 of EISCAT-3D, a VO handling protocol has been developed which allows Madrigal archives to be queried by a generic Virtual Observatory, in this case the UK's AstroGrid project. Essentially this amounts to putting a DSA around Madrigal, to allow the archives to be queried and accessed using standard VO queries.

Doing this has a two-fold benefit. Firstly, it allows the underlying archive to be based on the Madrigal system and the CEDAR data format, both of which are very familiar to the Solar-Terrestrial Physics community. However, it also allows the full functionality of the archive to be accessed by a new class of user, not familiar with the details of specific data formats, but only with the more generic skills of using a Virtual Observatory. As use of the VO evolves, we expect this type of user to become

increasingly common, to the point where the user of the future will need only generic VO skills and need not be aware of the location or format of the data which they are using. As the uptake of Virtual Observatories becomes more widespread, we believe that most of our future users will be of this kind – indeed we expect the techniques of VO use to become so embedded in the scientific culture that the need to understand the specifics of individual archives will become confined to archive specialists. Certainly, if EISCAT-3D is to draw in new user communities without long heritage of incoherent scatter use, as must be our aim, generic access based on Virtual Observatories will become a requirement, rather than an optional extra.

As noted above, the applicability of the CEDAR format and the Madrigal database is not confined to incoherent scatter data, instead the format is sufficiently flexible to accommodate data from a wide range of instruments, including most of the instrument types suggested in this report as components of the “EISCAT-3D observatory”. This means that it should be possible to store most of the data from the instruments supporting EISCAT-3D in a data format which is very close to that used for the storage of the radar data. This would have obvious advantages for users working with the data, as well as providing a uniform interface to VO data queries, irrespective of instrument type.

We have also noted in this report that ionospheric modelling is an essential activity for EISCAT-3D and its supporting instruments in two respects. First, the combined instrument complement of EISCAT-3D will represent a major data resource, both for validating models and for constraining them by data assimilation. Secondly, results from the models will also be used to obtain additional parameters from EISCAT-3D data, particularly the “indirectly derived” parameters which cannot be extracted from the data alone, and for which modelled parameters need to be combined with the observed data.

In this respect, the model can be treated like another instrument in the EISCAT-3D ensemble. Model output can be held in the database and, since the model outputs will be multiple parameters as a function of time and altitude, they can be formatted in the same way as the instrument data, with appropriate identification codes being used to mark them out as model output. Of course, one key requirement regarding the storage of model data is that the assumptions made in each model run should be carefully preserved. This is also the case with instrument data, where the instrument has multiple modes of operation, and emphasises the need for the EISCAT-3D database to have a very good capability for handling metadata – see the next section.

## **8. Metadata in EISCAT-3D**

As we have seen, the EISCAT-3D central archive will comprise a number of different data types. The dominant data set (in terms of volume) will consist of correlated data from the radars themselves – and this is certain to be highly flexible in form, since the type of correlation functions will depend on the precise experiment being performed, to the extent that the data set might not even be intelligible unless the details of the experiment are carefully preserved. The storage of data from the radar will involve not only conventional incoherent scatter data, but also data from the interferometry system, probably in the form of processed brightness functions. In principle, the possibility exists to use multiple different interferometric configurations in EISCAT-

3D, e.g. by applying different methods of splitting the central core array into different interferometric sub-sections, see the deliverables of Work Package 5. This means that the meta-data from both the incoherent scatter and interferometric parts of the system will be quite complex because the structure and content of these data will depend critically on the way in which they were created, and there is a wide range of different possibilities.

Similarly, a number of the instruments mentioned earlier in this report are capable of multiple different modes of operation (e.g. radars with different scans, sounders with different modulation schemes and multiple receiver configurations, or optical instruments with multiple filters). In these cases too, incorrect assumptions about the operating modes during a particular operation have the potential to result in profound mistakes in the interpretation of the data, and again call for complex metadata.

Because of this, there is a strong requirement for data in the central archive to be associated with high-quality metadata from each of the instruments (or models) concerned. The specification of these metadata, at least for the radar, is the responsibility of the monitoring and control work package (WP7), however their storage and association with the data is a WP8 responsibility.

Ideally, the metadata standard selected for EISCAT-3D would be similar to those which inform the choice of analysed data format, i.e. a standard which is well-known in the community and has wide applicability across different classes of instrument, as the Madrigal format does for analysed incoherent scatter and other instrument data. One problem is that, while there is a well-developed heritage in the development of data formats for solar-terrestrial physics, much less work has been done in producing a consistent system for encapsulating STP metadata.

An important challenge in providing metadata is the need to define the meaning of any given variable, not only data variables, but also including the status information which defines how the data were taken. This challenge is encapsulated in the idea of “ontologies” which, in computing terms, describe entities and the relationships between them. Ontologies are a key concept in underpinning internet search algorithms such as Google and are widely used in the commercial sector. In recent years, a number of attempts have been made to develop formal ontologies for space physics, but there is still no system which has gained general community acceptance.

The EU, under its Framework 7 programme, has recently announced funding for HELIO, a new virtual observatory programme for solar and solar-terrestrial physics, which partly builds on the foundations of EGSO (the European Grid for Solar Observations) funded under EU FP5. The HELIO consortium brings together a number of European developers and database specialists in the Solar/STP area, including members with experience of developing the SPASE system, a space science ontology from the USA which has been developed as a standard for NASA. A key aim of HELIO is to extend the accepted set of ontologies in space physics, and RAL (which leads Work Package 8 of the EISCAT-3D design study) is part of the HELIO consortium.

Given the relative lack of development of metadata and ontology standards in space physics up to now, it seems premature to specify the metadata system for EISCAT-3D

at this stage. It is also not appropriate for us to develop our own standard at this stage, since we aspire to use a standard which has widespread community acceptance. As a result, we have not yet spent a great deal of effort focusing on ontologies and metadata standards for EISCAT-3D. Instead we will work together with the HELIO consortium, whose studies are likely to be substantially complete by the time that construction of the EISCAT-3D data system actually begins, in the belief that this consortium can make substantial progress in improving the current situation.

## **9. Data, Users and Services**

In this report, we have examined in considerable detail the kinds of supporting instruments which we would expect to contribute data to the EISCAT-3D permanent central archive, in addition to the data from the EISCAT-3D radars themselves, whose form and content were dealt with in Deliverable 8.3. On this basis, we are now in a position to make a comprehensive list of all the data which we would expect to be held in an EISCAT-3D central archive which obtained data from a multi-instrument observatory-type facility of the kind which we envisage for EISCAT-3D.

We can expect these data to be at three levels. At “Level 1” comes the large set of bandpassed lag profile data (or, on occasion, sample-level data) from the EISCAT radars themselves. We refer to these as “level 1” data because they do not, in themselves, represent a data set with which a user can immediately do science – they have to be post-processed by data analysis software. With a complex instrument such as an incoherent scatter radar there is an obvious need to archive data at this level because of the great flexibility with which it can be treated afterwards, particularly in the case of the sample level data. In other words, if the data were not stored at this level, considerable post-processing flexibility would be lost, which cannot be recovered. While some of the supporting instruments also produce “level 1” data, these data are in most cases handled by their own internal data processing systems and not routinely archived. Exceptions are individual echo data (e.g. phase and angle-of-arrival) from ionospheric sounders with distributed receivers) and correlation functions from coherent scatter radars.

Most of the instruments contributing data to the EISCAT-3D central archive produce “Level 2” data sets – the kind which a scientist could immediately begin to use in scientific studies. Examples include plasma parameters from incoherent scatter radars, echo strength, spectral width and Doppler shift from other kinds of radars, ionograms and magnetograms, cosmic noise measurements from riometers, and images from optical systems.

Above this, there exists a third level of data, produced by combining together the “level 2” data products from multiple instruments. This kind of data combination was discussed in Section 7 of this report, and produces “value added” parameters which cannot be obtained from one instrument alone. Also included in this “level 3” data are the outputs of models which are driven using level 2 input data. These model outputs can be extremely valuable products in themselves though, as specified in the previous section, considerable care is needed in describing the metadata so that the conditions under which the model output was created can be completely defined.

Tables 9.1, 9.2 and 9.3 give one possible scenario for the complement of data products at each level in the EISCAT-3D archive, together with an estimate of their cadence and size and the instruments involved in producing them. In each column, the estimates are only specified to an order of magnitude, but the tables are illustrative of the data sets which will drive the growth of the archive. It is obvious that, not surprisingly, the growth rate of the archive is driven by the size of the lowest level data products (i.e. auto-correlated data from EISCAT-3D, interferometric data from EISCAT-3D and auroral images, especially where the instruments are capable of high temporal and spatial resolution).

Also not surprisingly we assume that data formats will become more standardised as the level of data products becomes higher. While auto-correlated and interferometry data from EISCAT-3D is best stored in binary forms which will probably be somewhat proprietary, a high degree of commonality in format will be present by for the level 2 archive products, with imager data capable of being stored in a common format for a variety of instruments and data from certain other instruments such as ionosondes and GPS receivers probably being best left in the formats most familiar to their respective communities, where substantial software exists to work with them. At the highest level it becomes increasingly obvious that data products should be encoded in a format such as Madrigal, which we use here as a short-hand for a standard binary system for encoding 2-d and 3-d data products.

Remember that, unlike the ring buffers, where the level of complexity of a set of data is often related to its longevity, all the data in the central archive will be permanently stored irrespective of level. No doubt other, more complex data products are also possible, but at some point it is appropriate to limit the number of parameters which EISCAT-3D will produce, not only for practical reasons associated with the availability of storage, but because the key aim of the archive is that it should be as open as possible to allow worldwide users to extract data products, in order to use them for their own scientific studies, including the creation of new data products.

EISCAT-3D Central Archive: Level 1 data				
Instrument	Data Set	Cadence	Size (GB/day)	Format
EISCAT-3D central site	Ion line lag profile matrices	1s	~100	Binary
EISCAT-3D remote sites	Ion line lag profile matrices	1s	~10 /beam	Binary
EISCAT-3D central site	Plasma line lag profile matrices	1s	~100	Binary
EISCAT-3D remote sites	Plasma line lag profile matrices	1s	~10 /beam	Binary
Coherent scatter radars	Correlation functions	10s	~1	Binary
MST/Meteor radars	Coherent IQ data	10s	~1	Binary
HF Doppler	Frequency spectra	1s	~1	Binary
FPI	Interference fringes	10s	~10	Binary

*Table 9.1: EISCAT-3D Central Archive: Level 1 Data Products*

EISCAT-3D Central Archive: Level 2 data				
Instrument	Data Set	Cadence	Size (GB/day)	Format
EISCAT-3D	Derived plasma parameters	10s	<<1	Madrigal
EISCAT-3D Interferometry	Brightness functions	10s	~10	Binary
EISCAT-3D	Velocity vectors	10s	<<1	Madrigal
Coherent scatter	RTI data	10s	<<1	Madrigal
Coherent scatter	Velocity data	10s	<<1	Madrigal
MST/Meteor radars	Radial data	10s	~1	Madrigal
MST/Meteor radars	Cartesian data	10s	<<1	Madrigal
Advanced sounder	Ionograms, phase and angle of arrival	10s	~1	Binary
Advanced sounder	Drift velocity	10s	<<1	Madrigal
Standard sounder	Ionograms	10s	<<1	Binary
HF Doppler	Gravity wave parameters	10s	<<1	Madrigal
Lidar	Backscattered power	10s	<<1	Madrigal
Lidar	Spectral width	10s	<<1	Madrigal
Lidar	Doppler velocity	10s	<<1	Madrigal
All-sky imager	Auroral images	1s	~10	Binary
High-resolution camera	Auroral images	1s	~100	Binary
Spectrometer	Multi-wavelength images	1s	~10	Binary
Airglow imager	Airglow images	10s	~10	Binary
FPI	Neutral wind fields	10s	<<1	Madrigal
Photometer/Radiometer	Intensity per frequency	1s	<<1	Madrigal
GPS receiver	RINEX files	1s	<<1	Rinex
Riometer	Noise intensity measurements	1s	<<1	Madrigal
Riometer	QDC-corrected absorption	1s	<<1	Madrigal
VLF/ELF Receiver	Spectra	1s	~1	Binary
Magnetometer	Tri-axial field data	0.1s	<<1	Madrigal

Table 9.2: EISCAT-3D Central Archive: Level 2 Data Products

EISCAT-3D Central Archive: Level 3 data				
Instrument	Data Set	Cadence	Size (GB/day)	Format
EISCAT-3D, coherent radars and advanced sounders	Plasma velocity field	10s	<<1	Madrigal
EISCAT-3D, coherent scatter radars and magnetometers	Potential patterns	10s	<<1	Madrigal
EISCAT-3D and FPIs	Ion-neutral difference velocity field	10s	<<1	Madrigal
MST/Meteor radars	Mesospheric velocity field	10s	<<1	Madrigal
Physics-based model	Nominal background ionosphere and neutral atmosphere	100s	<<1	Madrigal
Assimilative model	Corrected background ionosphere and neutral atmosphere	100s	<<1	Madrigal
EISCAT-3D, FPIs, coherent scatter radars and magnetometers	Electrodynamic parameters	10s	<<1	Madrigal
EISCAT-3D, models	Heat flux	10s	<<1	Madrigal
EISCAT-3D, models	Suprathermal electron flux	10s	<<1	Madrigal
EISCAT-3D, auroral imagers, riometers	Characteristic energy maps	10s	<<1	Madrigal
EISCAT-3D, GPS and beacon satellite data, modelling	Ionospheric tomographic images	10s	~10	Binary

*Table 9.3: EISCAT-3D Central Archive: Level 3 Data Products*

It should be mentioned here that we expect to have at least two kinds of users for the EISCAT-3D system. Obviously the core aim of the facility is to serve an active scientific community whose priority is to gain increased understanding of energy flow in the upper atmosphere, the connection between the atmosphere and the geospace environment and the coupling between the various atmospheric layers. However, we also expect a new class of “service users” which does not really exist in the present EISCAT system. We envisage that these will be users in communities such as global positioning, navigation, orbit prediction and communications, who will not be specialists in the interpretation of radar data, but will come to EISCAT seeking “value added” (mainly level 3) products to use in their own applications. Work Package 10 of the design study (novel uses of incoherent scatter) has applied some effort into identifying such user communities and understanding their needs – for details see their deliverables. We are also working together with the European consortium developing the EURIPOS project, a large multi-national collaboration geared to the provision of space weather services in Europe, which will propose for EU funding in late 2009 or 2010, with EISCAT being one of the partners in the study. Although this

collaboration is presently at an early stage, we hope it will lead on to the development of products and services which will ultimately form part of the EISCAT-3D data system.

## **10. Summary and Conclusions**

In this deliverable, we have introduced the concept of EISCAT-3D as a multi-instrument observatory, based on the concept of a multistatic phased array with one large central site and four passive remote arrays, two of which are optimised for studies of E-region or middle atmosphere dynamics and two for F-region and upper atmosphere dynamics. Based upon a survey of supporting diagnostics being operated elsewhere in the world, we have proposed a state of the art complement of supporting instruments to be clustered at each site, consistent with the idea that two of the remote sites should be “radio quiet” to offer the best conditions for passive instruments. Only supporting instruments which do not require regular human interaction are considered for deployment at the remote sites, as these sites are envisaged for long-term unattended operations.

We have then examined the data rate requirements for the proposed instrument complement, showing that at the central site some instruments can be directly connected to the central archive, while others require an intermediate connection to the local ring buffer, in order to allow their data volumes to be reduced by pre-processing. In comparison to the data rates flowing into and out of the ring buffers from the EISCAT-3D radars themselves, the data rates from the supporting instruments are completely trivial, and the required pre-processing is not complex.

At the remote sites, we suggest that all supporting instruments should be connected to the ring buffer, whether or not they have an additional direct connection to the central archive. This allows all of the supporting data to be routed to the ring buffer during times when the network connection is unavailable. The size of the ring buffer relative to the size of the supporting data sets makes it possible to store such data for quite long periods.

We have shown that, in contrast to the EISCAT-3D raw data, which can be quite heavily decimated before archiving, the data from the supporting instruments cannot be reduced in volume by the same extent, so that although the impact on the ring buffers is negligible, the impact on the size and growth rate of the central archive is about 25%, compared to what would be the case if the supporting instruments were not present. We consider this a very acceptable overhead for the additional science return.

Finally we have examined the possible uses that can be made of the supporting data, either by combining data from different instruments together, combining them with data from EISCAT-3D or ingesting them into models. We show that it is possible to generate a range of data products which are likely to be of interest to the science community and have the potential to provide service-type inputs to applications users.

In our next (and final) deliverable from Work Package 8, we will discuss the interfaces needed for users and services to interact with the EISCAT-3D data system at a variety of levels. These interfaces constitute the so-called “access layer” of the

data system. We will also report on the implementation of a real-world database system fitted around the present EISCAT data archive in Kiruna using computers provided by the Rutherford Appleton Laboratory, the lead partner in Work Package 8.

## **References:**

- Aponte, N., M. P. Sulzer, M. J. Nicolls, R. Nikoukar, and S. A. González (2007), Molecular ion composition measurements in the *F1* region at Arecibo, *J. Geophys. Res.*, 112, A06322, doi:10.1029/2006JA012028
- Baddeley L.J., T. K. Yeoman, and D. M. Wright. HF doppler sounder measurements of the ionospheric signatures of small scale ULF waves, *Annales Geophysicae*, 23, 1807–1820, 2005
- Baggeley W.J., R.G.T. Bennett, D.I. Steel and A.D. Taylor, The Advanced Meteor Orbit Radar Facility (AMOR), *Q. J. Roy. Astr. Soc.*, 35, 293-320, 1994
- Belova E., S. Kirkwood, J. Ekeberg, A. Osepian, I. Haggstrom, H. Nilsson and M. Rietveld, The dynamical background of polar mesospheric winter echoes from simultaneous EISCAT and ESRAD observations, *Ann. Geophys.*, 23, 1239-1247, 2005
- Bjørnå N. and T Hansen, Effect of a Power Law Particle Flux on the Ionospheric Incoherent Scattering Cross Section, *Phys. Scr.* 33 284-288 doi: 10.1088/0031-8949/33/3/017, 1986
- Calhoun R., R. Heap, M. Princevac, R. Newson, H. Fernando and D. Ligon, Virtual towers using coherent Doppler lidar during the Joint Urban 2003 Dispersion Experiment, *J. Climate App. Meteor.*, 45, 1116-1126, 2006
- Chernogor et al, Variations in HF Doppler spectra measured at vertical incidence, Paper No. 143, Proceedings of the 2002 URSI General Assembly, 2002
- Conde M. and R.W. Smith, Mapping thermospheric winds in the auroral zone, *Geophys. Res. Lett.*, 3019-3022, 1995
- Friedrich M., G. Egger, L.A. McKinnell and E. Belova, Perturbations in EISCAT electron densities visualised by normalisation, *Adv. Space Res.*, 38, 2413-2417, 2006
- Kosch M.J., T. Hagfors and K. Schlegel, Extrapolating EISCAT Pedersen conductances to other parts of the sky using ground-based TV auroral images, *Ann. Geophys.*, 16, 583-588, 1998
- Lind F., et al, First passive radar observations of auroral E-region irregularities, *Geophys. Res. Lett.*, 26 (14), 2155-2158, 1999
- Lunde J., B. Gustavsson, U.P. Lovhaug, D.A. Lorenten and Y. Ogawa, Particle precipitations during NEIAL events: simultaneous ground-based observations at Svalbard, *Ann. Geophys.*, 25, 1323-1336, 2007
- Reinisch B.W., Modern Ionosondes, pp440-458 in *Modern Ionospheric Science*, edited by H. Kohl, R. Ruster and K. Schlegel, European Geophysical Society, 37191 Katlenburg-Lindau, 1996

Ruohoniemi J.M. and K.B. Baker, Large-scale imaging of high-latitude convection with SuperDARN auroral radar network HF radar observations, *J. Geophys. Res.*, 103, 20, 797-807, 1998

Sullivan J.M., M. Lockwood, B. S. Lanchester, E. P. Kontar, N. Ivchenko, H. Dahlgren, and D. K. Whiter An optical study of multiple NEIAL events driven by low energy electron precipitation, *Ann. Geophys.*, 26, 2435-2447, 2008

Titheridge (1993) "Computer-controlled operation of the IPS-42 ionosonde" in *Proceedings of Session G6 at the 24<sup>th</sup> URSI General Assembly, Kyoto, Japan*, editor Phil Wilkinson.

Toyamatsu et al, proceedings of the 33<sup>rd</sup> Annual European Meeting on Atmospheric Studies by optical methods, *IRF Science Report*, 292, 75-84, 2008

Trondsen T.S., *The Campaign Mode: An essential tool for auroral microphysics*, presented at the International Symposium on KuaFu (2002)

Webster A.R., P.G. Brown, J. Jones, K.J. Ellis and M. Campbell-Brown, *The Canadian Meteor Orbit Radar (CMOR)*, *Atmos. Chem. Phys. Discuss.*, 4., 1181-1204, 2004

Weimer D.R., A flexible IMF-dependent model of high-latitude electric potentials having "space weather" applications, *Geophys. Res. Lett.*, 23(18) 2549-2552, 1996

Wright J.W and M.L.V. Pitteway, Real-time data acquisition and interpretation capabilities of the Dynasonde, 1: Data acquisition and real-time display, *Radio Sci.*, 14, 815-825, 1979a

Wright J.W and M.L.V. Pitteway, Real-time data acquisition and interpretation capabilities of the Dynasonde, 2: Determination of magneto-ionic mode and echo location using a small spaced receiver, *Radio Sci.*, 14, 827-835, 1979b